ADVANCED HEALTHCARE MATERIALS
www.advhealthmat.de

Recent Advances in "Functional Engineering of Articular Cartilage Zones by Polymeric Biomaterials Mediated with Physical, Mechanical, and Biological/Chemical Cues"

Dorsa Dehghan-Baniani, Babak Mehrjou,* Paul K. Chu,* Wayne Yuk Wai Lee,* and Hongkai Wu**

Articular cartilage (AC) plays an unquestionable role in joint movements but unfortunately the healing capacity is restricted due to its avascular and acellular nature. While cartilage tissue engineering has been lifesaving, it is very challenging to remodel the complex cartilage composition and architecture with gradient physio–mechanical properties vital to proper tissue functions. To address these issues, a better understanding of the intrinsic AC properties and how cells respond to stimuli from the external microenvironment must be better understood. This is essential in order to take one step closer to producing functional cartilaginous constructs for clinical use. Recently, biopolymers have aroused much attention due to their versatility, processability, and flexibility because the properties can be tailored to match the requirements of AC. This review highlights polymeric scaffolds developed in the past decade for reconstruction of zonal AC layers including the superficial zone, middle zone, and deep zone by means of exogenous stimuli such as physical, mechanical, and biological/chemical signals. The mimicked properties are reviewed in terms of the biochemical composition and organization, cell fate (morphology, orientation, and differentiation), as well as mechanical properties and finally, the challenges and potential ways to tackle them are discussed.

1. Introduction

Articular cartilage (AC), a 2–4 mm thick hyaline cartilage that covers the epiphyseal surface of joints, provides low-friction articulation to facilitate load transmission to the subchondral bone due to the extraordinary viscoelastic properties.[1] Each zone in the hyaline cartilage has its own features and biological functions. Lubrication and painless slipping of joints originate from the superficial zone (SZ) while the middle zone (MZ) is responsible for transfer of the applied load to the SZ toward the bottom layers of the cartilage. Moreover, the deep zone (DZ) beside the calcified cartilage (CC) is responsible for load passing and connection to the subchondral tissue. Hyaline cartilage is an aneural connective tissue with low cell density that can be damaged by trauma, inflammation, aging, and degenerative joint diseases like osteoarthritis. Insufficient supply of blood, stem/progenitor cells, and nutrients to the damaged cartilage tissues owing

D. Dehghan-Baniani, H. Wu
Department of Chemical and Biological Engineering Division of Biomedical Engineering
The Hong Kong University of Science and Technology
Hong Kong China
E-mail: dorsadehghanbaniani@cuhk.edu.hk; chhkwu@ust.hk

D. Dehghan-Baniani, W. Y. W. Lee
Musculoskeletal Research Laboratory
SH Ho Scoliosis Research Laboratory
Department of Orthopaedics and Traumatology
Faculty of Medicine
The Chinese University of Hong Kong
Hong Kong SAR China
E-mail: waynelee@cuhk.edu.hk

D. Dehghan-Baniani, W. Y. W. Lee
Li Ka Shing Institute of Health Sciences
The Chinese University of Hong Kong
Prince of Wales Hospital
Hong Kong SAR China

B. Mehrjou, P. K. Chu
Department of Physics
Department of Materials Science and Engineering
and Department of Biomedical Engineering
City University of Hong Kong
Kowloon, Hong Kong China
E-mail: bmehrjou2-c@my.cityu.edu.hk paul.chu@cityu.edu.hk

W. Y. W. Lee
Joint Scoliosis Research Centre of the Chinese University of Hong Kong and Nanjing University
The Chinese University of Hong Kong
Hong Kong SAR China

W. Y. W. Lee
Center for Neuromusculoskeletal Restorative Medicine
CUHK InnoHK Centres
Hong Kong Science Park, Hong Kong SAR China

H. Wu
Department of Chemistry and the Hong Kong Branch of Chinese National Engineering Research Center for Tissue Restoration
The Hong Kong University of Science and Technology
Clearwater Bay, Kowloon, Hong Kong SAR China

The ORCID identification number(s) for the author(s) of this article can be found under https://doi.org/10.1002/adhm.202202581

DOI: 10.1002/adhm.202202581

to the avascularity and limited proliferation and migration capabilities of mature chondrocytes are the main reasons for slow turnover of the cartilage extracellular matrix (ECM),[1–6] which is further challenged by the anisotropic nature and unique structural organization with unique biochemical and biomechanical properties.

Surgical approaches such as microfracture, debridement, partial meniscectomy, and tibial osteotomy have been used clinically, but their outcomes, particularly cartilage tissue repair/regeneration remain unsatisfactory.[7] For example, they often result in fibrocartilage formation which lacks the durability, microstructure, and load-bearing properties of a healthy hyaline cartilage.[8] This fibrocartilage is substantially different from hyaline cartilage specifically regarding zonal configuration, thus not favorable for long-term daily activities. While scientists have been searching for new cartilage treatment methods,[9–12] they have been also focused on improving the outcomes of currently used surgical techniques. For example, incorporation of chitosan hydrogel (BST-CarGel) with the blood originating from microfracture operation provides better stability to newly formed tissues in phase II of the clinical trial.[13–15] The other limitations of the current clinical approaches include donor-site morbidity, lack of suitable donors, immune rejection, graft instability, invasiveness of surgical procedures, and disappointing long-term efficiency.[16] Accordingly, in many cases, total joint replacement is the ultimate option despite difficulties including the limited in vivo lifespan of implants.[17,18]

Given the drawbacks associated with current interventions, tissue engineering (TE) of AC has provided tremendous, advanced alternatives in this field.[19,20] Employing this approach can be game changing as it has the potential to restore the zonal configuration and thus the full functionality of the lost AC.[21] Cartilage TE is a promising approach wherein scaffolds with or without cells and bioactive molecules are designed to produce functional cartilages.[22–27] In this method, biomaterials are indispensable and must be able to withstand chemical and mechanical treatments and be processed into structures with the suitable surface chemistry as well as biological, physical, and mechanical properties according to needs. Considering the capability of biopolymers to be chemically and physically modified to tune the aforementioned properties like morphologies, porosities, surface-to-volume ratios, swelling, and biodegradation rates along with their processability to develop films, sponges, scaffolds, and hydrogels, they have been employed in various TE applications.[28,29]

Generally, scaffolds should offer sufficient porosity through interconnected pores with the appropriate size to accommodate cell attachment, proliferation, and migration as well as satisfactory nutrient diffusion. They must also possess acceptable cytocompatibility while providing a controllable degradation rate matching that of neo-cartilage formation.[30,31] They may be loaded with signaling biomolecules and drugs for defect management and cartilage regeneration. Since these matrices are implanted or injected into defects, they must be sufficiently sturdy to be handled by surgeons. Scaffolds can be incorporated with cells such as chondrocytes, multipotent mesenchymal stromal cells, and stem/progenitor cells before implantation/injection or for a period of in vitro culture up to weeks before transplantation.[3] Although cell-based therapies are more complicated than implanting acellular matrices, they are believed to provide better/accelerated tissue regeneration and remodeling by inducing extracellular matrix (ECM) deposition and secreting regenerative factors in the defects.[32–34] Moreover, the cartilage immune nature arising from the dense ECM and avascularity paves the road for utilizing allogenic cells in scaffolds without the need to use immunosuppressants.[35]

A successful cartilaginous construct should be able to integrate with both the subchondral bone and adjacent cartilage as required for mechanotransduction and proper load distribution. Therefore, the mechanical properties should be the same as those of adjoining cartilage, otherwise it could be prone to degradation because of strain mismatch. It should be resilient enough under loading which can be achieved by the unique zonal microarchitecture of the native cartilage. Furthermore, the composition ought to replicate that of the native cartilage ECM to deliver to cells biologically relevant signals while withstanding the inflammatory environment of injured tissues.[18,36–38] Nevertheless, despite advances pertaining to cartilage TE in the past 20 years, very few orthopedic products have reached the market.[39] Therefore, to develop effective functional bioscaffolds for cartilage restoration that can totally mimic the inherent properties of the native cartilage, the zonal configuration of AC should be considered and designed more realistically. This is because the AC optimal performance originates from the distinct functions of its layers which in turn arise from their unique composition, structure, and the associated mechanical properties.

Accordingly, this review focuses on polymeric-based biomaterials designed for functional engineering of AC zones. An overview of AC zonal organization is presented in terms of the microstructure, composition, and functions which should be considered when designing scaffolds. The exogenous stimuli-assisted layered organization of cartilages in biopolymeric constructs is described and important results from the past decade are summarized. Finally, recommendations are proposed to enable development of better polymeric scaffolds for the repair of AC layers.

2. Articular Cartilage Structure and Functions

The ECM of AC is dense and considered as a biphasic composite embedded with sparsely distributed chondrocytes. It consists of an organic solid matrix made of the fibrillar collagen network (mainly type-II, Col II) filled with glycosaminoglycans (GAGs), proteoglycans (PGs), and a lesser amount of glycoproteins, all of which are saturated in a liquid phase composed of water (70–80% by weight) and mobile ions (Ca^{2+}, K^{+}, Cl^{-}, Na^{+}).[1,40,41] The stiff and elastic crosslinked collagen network (fiber diameters: 50–300 nm) provides the cartilage shape and strength to resist lateral expansion upon axial compression. PGs such as aggrecan and sulfated-GAGs (sGAGs) that bind to collagen fibers maintain the large water and ion contents through negative charges and offer unique load bearing properties.[3,42]

Histologically, AC ECM consist of four different layers based on the ultrastructure and functions, namely the SZ, MZ, DZ, and calcified zone (CZ) as mentioned before (**Figure 1**). The structure, ECM composition, metabolic activity, density of chondrocytes, morphology, and organization across the AC depth are described in the following sections.[4]

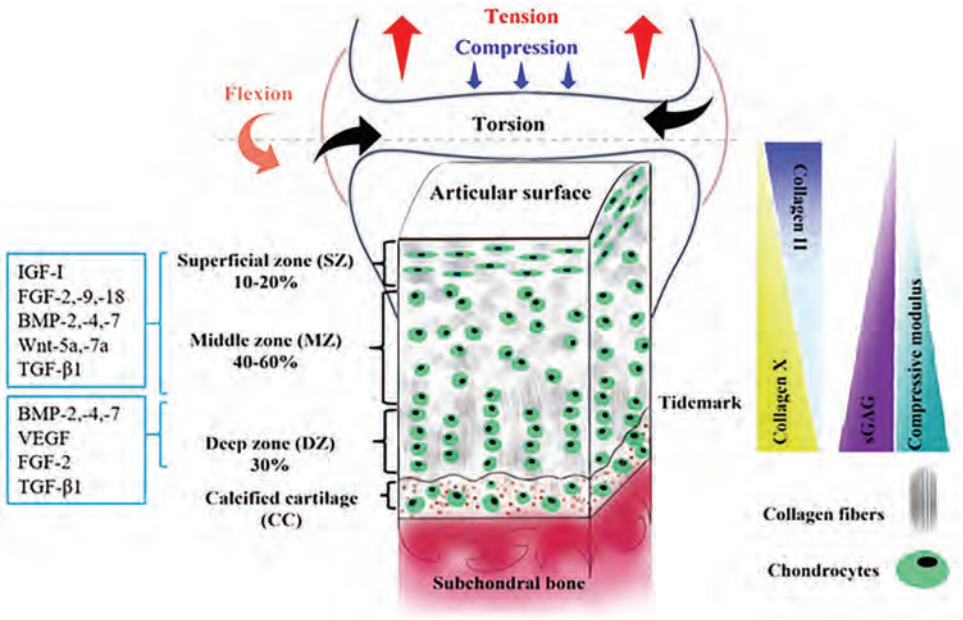

Figure 1. Schematic illustration of the AC layers; SZ, MZ, DZ, and CZ with zone-dependent ECM composition, collagen fiber orientations, and cell alignment and morphology. The GFs governing the chondrocytes are categorized based on the stage of chondrocyte lineage.

2.1. Superficial Zone

The SZ or tangential zone comprising almost the first 10–20% of the AC thickness is located right under the surface adjacent to both the synovial fluid and MZ (Figure 1). It provides a frictionless gliding surface and protects the deeper zones from shear stress by densely packed collagen fibers (primarily type-II and IX) aligned parallel to the joint surface. It facilitates dissipation of high tensile and compressive stresses during articulation.[43] While the collagen fibrils are thinner in this region, they possess the biggest collagen content, low levels of aggrecan and the smallest compressive modulus compared to other layers (≈25 times more deformability than the middle region).[32,44] Therefore, the integrity of this layer is of great importance as it functions as a filter for large macromolecules and segregates the deeper zones from the synovial immune system. If disrupted, the mechanical properties of the cartilage will deteriorate leading to rapid cartilage wearing and breakdown. It is the first layer that shows degenerative alterations in osteoarthritis development.[5]

The superficial layer has a relatively large density of flattened and disc-shape chondrocytes which are clustered horizontally. It has a small density of PGs attached to the collagenous membrane that effectively resists fluid flow out of the cartilage upon compression.[5] Fibril related decorin and biglycan exist in higher concentrations in this region. SZ chondrocytes exclusively express clusterin which is a glycoprotein that controls cell death and complement activation. Besides, they express SOX-9 which is a pre-chondrogenic marker as well as the lubricating protein proteoglycan 4 (PRG4)/superficial zone protein (SZP) also known as lubricin which functions as a boundary lubricant by abating wear and friction.[1,4,45,46] The SZ has the highest fibroblast growth factor (FGF) which declines by depth.[21]

Since the superficial layer tolerates the maximum load, attention needs to be paid to the mechanical properties of the substitutes in this region. Figure 1 also illustrates that the growth factors (GFs) govern chondrocytes which are categorized based on the stage of chondrocyte lineage.[47]

2.2. Middle Zone

The MZ (transitional zone, TZ) is located immediately under the SZ and in contact with the DZ. The thicker collagen fibers in this region are oriented randomly and packed loosely to form a backbone for water retention in the matrix when combined with larger PGs contents. The aggrecan content in the MZ reaches the maximum level[5,44,48] and TZ covers 40–60% of the overall AC thickness that is populated with low-density spherical chondrocytes. Moreover, hyaluronic acid (HA) and collagen type-II are highly expressed by the pre-hypertrophic chondrocytes in this layer.[46] It possesses a higher compressive modulus than the tangential layer, thereby providing more resistance to the compression applied to joints.[31,44] Functionally, this layer provides the transition between the SZ shear force and deeper zone compressive force.[49]

2.3. Deep Zone

Nearly 30% of AC is the DZ which is also termed as the radial zone due to the radially arranged components. It is a dense PG-rich matrix (highest amount of PGs among all the layers) with the thickest collagen fibrils aligned perpendicular to the articulating surface to distribute the load and display the highest resistance to compressive stress. The DZ has the smallest water content and chondrocyte population that is large and spheroidal and typically orientated in a columnar arrangement parallel to the collagen fibrils.[44,49]

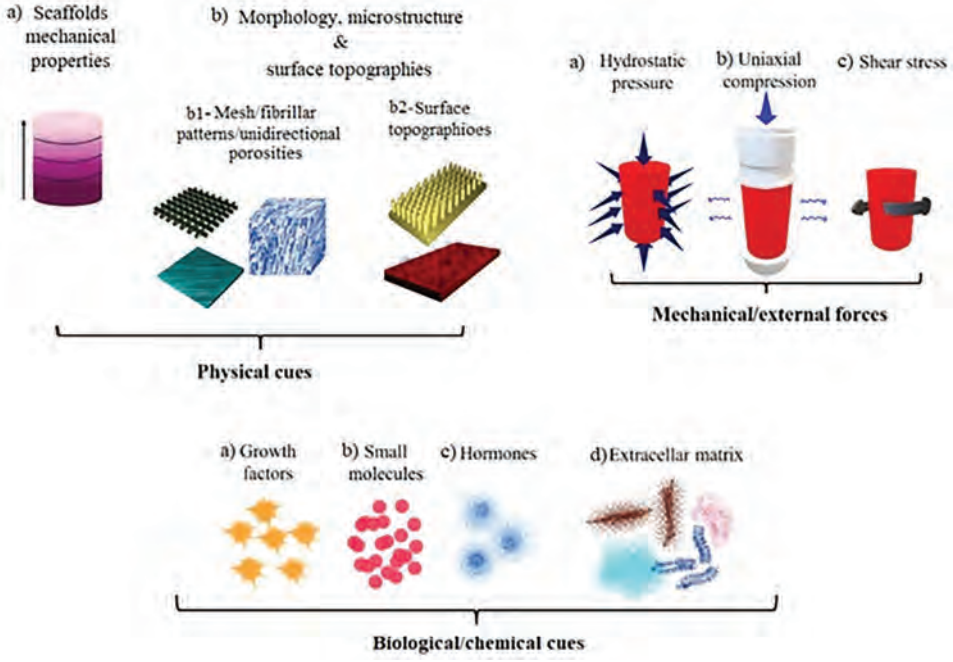

Figure 2. Schematic illustration of the exogenous stimuli including the physical cues, mechanical forces, and biological/chemical signals for cartilage TE.

2.4. The Calcified Zone

The CZ is separated from the DZ by a tidemark, revealing a transition to the stiff subchondral bone. It is called CC because of mineralization that delivers a smooth transition of mechanical properties between the cartilage and subchondral bone by redistributing mechanical forces at the interface. Chondrocytes in this region are scarce and small, possessing hypertrophic phenotype and nearly no endoplasmic reticulum. In some parts, chondrocytes are surrounded by calcified matrix, demonstrating a very low metabolic activity.[44,50]

CZ plays an essential role in anchoring the cartilage to bone[51] via securing the DZ collagen fibers to the subchondral bone by hydroxyapatite (HAp) crystals.[1] This region acts as a barrier for blood diffusion from the underlying bone to hyaline cartilage through which the interstitial fluid can be transferred to each layer. Considering the hypoxic microenvironment in the cartilage which governs the cell growth and tissue repair, the CZ lower permeability is vital for stabilizing such required physiological condition inside the cartilage.[49,50] The hypertrophic chondrocytes in the CZ express alkaline phosphatase (ALP) and collagen type-X and osteocalcin.[46]

The significant role of each layer for proper functioning of AC requires biomaterials that can replicate the AC zonal arrangement with anisotropic properties by TE approaches. Recent progress in bioscaffolds for cartilage TE have been reviewed.[3,4,16,32,35] Among the various types of biomaterials used for this purpose, biopolymers have attracted substantial attention on account of the processability and flexible biophysical and biochemical properties. However, the biomimetic properties of engineered scaffolds are still not satisfactory in order to fully repair large cartilage lesions.

Here, we discuss the exogenous stimuli including physical, biological/chemical, and mechanical signals employed in biopolymeric scaffolds for regional organization of engineered AC (**Figure 2**). Selected published works in the past decade are summarized in **Table 1** to exemplify the exploitation of these stimuli in scaffolds to imitate AC zones and the mimicked properties in terms of the ECM composition, morphology, cell fate, and mechanical properties.

3. Exogenous Stimuli Assisting Zonal Organization of Cartilage in Biopolymeric Constructs

3.1. Physical Cues

Cells, regardless of whether they are pre-seeded on biomaterials or from the host tissues, sense physical cues in the peripheral environment such as the biomaterials stiffness, microstructure, and surface topography, which determine the cell fate and biological response.[23,52,53] Accordingly, attention must be paid to physical cues in designing microenvironmental niches that are recognized by cells. If the improper physical stimuli are exerted, undesired cell differentiation or delayed tissue healing may occur. In the following sections, these features are discussed in details.

3.1.1. Mechanical Properties of Biopolymers

The substrate stiffness can regulate the cellular morphology, fate, development, and differentiation substantially.[52,53] Generally, substrates with similar stiffness as native cartilage have

Table 1. Summary of the biopolymeric scaffolds developed in the past decade using exogenous stimuli for zonal cartilage TE together with the mimicked properties.

	Stimuli										Mimicked zone			Obtained mimicked properties						
	Physical cues			External mechanical forces			Biological/chemical cues													
Biopolymer	Mechanical properties	Morphology/microstructure	HP	Compression	Shear stress	CFs	Hormones	Small molecules	ECM	Superficial zone	Middle zone	Deep zone	Calcified zone	ECM deposition/gene expression	Mechanical properties	Physical properties	Cell morphology and orientation	Cell density/type	In vivo studies	Ref.
PCL-based bi-layered scaffold	✓	Fibrillar pattern								✓				Higher sGAG, Col I, II, and X, Higher ECM deposition	Frictionless, Tensile modulus: 28 ± 2 MPa, Compressive modulus: 140 ± 20 kPa	Aligned fibrillar pattern, reduced roughness, surface roughness: 3 ± 1 µm	—	Higher bovine chondrocytes density upon 4 weeks in vitro cell culture	—	[105]
												✓		Lower sGAG, Col I, II, and X, lower ECM deposition	Tensile modulus: 0.04 ± 0.02 MPa, Compressive modulus: 40 ± 5 kPa	Porous structure, Surface roughness: 16 ± 10 µm		Lower bovine chondrocytes density upon 4 weeks in vitro cell culture		
PCL-ALG-based tri-layered construct	✓	Lay-down filaments								✓				Lowest ECM deposition, lowest Col I, and X	Tensile modulus: 61.57 ± 2.05 MPa, Compressive modulus: 20.44 ±1.32 MPa	0/90° lay-down pattern, filament gap: 300 µm	Elongated cells along the PCL pattern	Low rat BMSCs density upon in vitro cell culture	—	[87]
											✓			Intermediate ECM deposition, highest Col I, and X	Tensile modulus: ≈38 MPa, Compressive modulus ≈ 9.5 MPa	0/60° lay-down pattern, filament gap: 500 µm	Elongated cells along the PCL pattern	Intermediate rat BMSCs density upon in vitro cell culture		
												✓		Highest ECM deposition, Highest Col II, and aggrecan	Tensile modulus: ≈22 MPa, Compressive modulus ≈ 6 MPa	0/30° lay-down pattern, filament gap: 700 µm	Elongated cells along the PCL pattern with highest cell area	High rat BMSCs density upon in vitro cell culture		
PCL-collagen based tri-layered scaffold	✓	Fibrillar pattern							Collagen	✓				-	Compressive modulus: 19.99 ± 3.40	Aligned fibrillar PCL, Fiber diameter: 1.20 ± 0.51 µm	—	—	—	[88]
											✓				Compressive modulus: 39.52 ± 15.34	Randomly orientated PCL Fibers, Fiber diameter: 2.00 ± 0.63 µm				
												✓			Compressive modulus: 136.77 ± 49.30KPa	Vertically-orientated PCL Fibers				
PLA-based tri-layered scaffold		Tubular porosities								✓				Intermediate sGAG	Compressive modulus: 0.008 ± 0.001 MPa	Tubular pores parallel to the surface, guided ECM deposition along the pores	Elongated chondrocytes along the tubular structure	Human fetal chondrocytes	—	[98]
											✓			High sGAG	Compressive modulus: 0.19 ± 0.04 MPa	Disorganized ECM morphology	Spherical chondrocytes			
												✓		HAp formation, Intermediate sGAG	Compressive modulus: 0.07 ± 0.007 MPa	Orthogonally oriented tubular pores to the surface	Elliptical shaped chondrocytes orientated in a columnar fashion			

(*Continued*)

Table 1. (Continued).

	Stimuli										Mimicked zone			Obtained mimicked properties					
	Physical cues			External mechanical forces		Biological/chemical cues													
Biopolymer	Mechanical properties	Morphology/microstructure	HP	Compression	Shear stress	GFs	Hormones	Small molecules	ECM	Superficial zone	Middle zone	Deep zone	Calcified zone	ECM deposition/gene expression	Mechanical properties	Physical properties	Cell morphology and orientation	Cell density/type	In vivo studies	Ref.
Cartilage-derived ECM hydrogel						TGF-β1, BMP7, IHH, IGF-1			Bovine cartilage ECM	✓				Higher SZP, Col II, and SOX-9	≈13 kPa elastic modulus	—	Rounded hMSCs	High hMSCs density	—	[168]
											✓			Higher aggrecan	≈13 kPa elastic modulus			Intermediate hMSCs density		
													✓	Higher Col X and ALP	≈13 kPa elastic modulus			Low hMSCs density		
PEG-based hydrogels combined with PLA nanofibers	✓	Fibrous patterns				TGF-β1, BMP7, IGF-1			HAp	✓				Highest SZP, Lowest GAG, and Col II	Compressive modulus: 80 KPa	—	Rounded hMSCs	hMSCs, 60×10^6 Cells per mL	—	[64]
											✓			Highest Col II and aggrecan, Intermediate GAG	Compressive modulus: 2.1 MPa			hMSCs, 20×10^6 Cells per mL		
													✓	Highest Col X, GAG, and mineral deposition	Compressive modulus: 320 MPa	Aligned PLA nanofibers perpendicular to the surface		hMSCs, 15×10^6 Cells per mL		
GelMA hydrogel combined with PCL-PEG-triblock polymer and PLGA microspheres	✓	Lay-down fibrous pattern				TGF-β1, BMP2, BMP7				✓				Highest SZP and SOX-9, high Col II	Highest lubrication, Compressive modulus: 283.6 ± 22.3 kPa	0–30° lay-down pattern, Fiber spacing: 100 µm	Aligned rabbit BMSCs along the long axis of fibers	Rabbit BMSCs	Rabbit osteochondral defect model	[42]
												✓		Highest CILP and aggrecan, high Col II	Compressive modulus: 256.6 ± 24.9 kPa	0–90° lay-down pattern, Fiber spacing: 200 µm	Irregular distribution of rabbit BMSCs with a perpendicular-dominant cell orientation trend	Rabbit BMSCs		

(*Continued*)

Table 1. (Continued).

Biopolymer	Stimuli: Physical cues: Mechanical properties	Stimuli: Physical cues: Morphology/microstructure	Stimuli: External mechanical forces: HP	Stimuli: External mechanical forces: Compression	Stimuli: External mechanical forces: Shear stress	Stimuli: Biological/chemical cues: GFs	Stimuli: Biological/chemical cues: Hormones	Stimuli: Biological/chemical cues: Small molecules	Stimuli: Biological/chemical cues: ECM	Mimicked zone: Superficial zone	Mimicked zone: Middle zone	Mimicked zone: Deep zone	Mimicked zone: Calcified zone	Obtained mimicked properties: ECM deposition/gene expression	Obtained mimicked properties: Mechanical properties	Obtained mimicked properties: Physical properties	Obtained mimicked properties: Cell morphology and orientation	Obtained mimicked properties: Cell density/type	Obtained mimicked properties: In vivo studies	Ref.
Agarose-based hydrogel							T3		HA				✓	High GAG, Col X, I, and II and mineral deposition	Compressive modulus: 27.1 ± 1.5 kPa, Dynamic shear modulus: 75.5 ± 8.5 kPa	—	Rounded chondrocytes with larger surface area compared to control	Chondrocytes isolated from bovine deep zone cartilage	—	[175]
PCL and PGS-based scaffold		Fibrous pattern						KGN		✓				High sGAG, SOX-9, Col II, ACAN, SZP	Tensile modulus: 11.8 ± 0.7 MPa	—	Non-spherical non-ellipsoidal hBMSCs	hBMSCs	—	[177]
Bi-layered scaffold based on Collagen, PLGA, Chitosan, HAS and Silk fibroin	✓	Tubular porosities				TGF-β1		KGN	Collagen, HAS	✓				Highest cartilaginous ECM deposition upon 16 weeks in vivo implantation of bi-layered structure	Compressive moduli of the whole scaffold: 1.2 kPa, High surface smoothness upon 16 weeks in vivo implantation	—	Uniformly aligned chondrocytes upon 16 weeks in vivo implantation of bi-layered scaffold	BMSCs	Rabbit knee osteoarthritic cartilage defect model	[178]
PEG-based gels combined with CS and HA	✓								HA, CS	✓				Highest Col II, lowest GAG	Compressive modulus: 209.1 ± 38.16 kPa	—	—	D1, mouse BMSCs	—	[188]
											✓			Intermediate Col II and GAG	Compressive modulus: 270.87 ± 31.559 kPa					
												✓		Lowest Col II, High GAG	Compressive modulus: 1227.93 ± 102.14 kPa					
													✓	Highest Col X	Compressive modulus: 68.18 ± 37.37 kPa					
PEG-based gels combined with CS, HA, MMP-pep	✓								HA, CS	✓				Lowest GAG and Col X, Highest Col I and II	Compressive modulus: 472.16 ± 141.77 kPa	—	—	D1, mouse BMSCs	—	[189]
											✓			Intermediate GAG, Col I, II, and X	Compressive modulus: 715.44 ± 215.49 kPa					
												✓		Highest GAG and Col X, lowest Col I and II	Compressive modulus: 1712.8 ± 248.33 kPa					

(*Continued*)

Table 1. (Continued).

Biopolymer	Stimuli: Physical cues: Mechanical properties	Stimuli: Physical cues: Morphology/microstructure	Stimuli: External mechanical forces: HP	Stimuli: External mechanical forces: Compression	Stimuli: External mechanical forces: Shear stress	Stimuli: Biological/chemical cues: GFs	Stimuli: Biological/chemical cues: Hormones	Stimuli: Biological/chemical cues: Small molecules	Stimuli: Biological/chemical cues: ECM	Mimicked zone: Superficial zone	Mimicked zone: Middle zone	Mimicked zone: Deep zone	Mimicked zone: Calcified zone	Obtained mimicked properties: ECM deposition/gene expression	Obtained mimicked properties: Mechanical properties	Obtained mimicked properties: Physical properties	Obtained mimicked properties: Cell morphology and orientation	Obtained mimicked properties: Cell density/type	Obtained mimicked properties: In vivo studies	Ref.
Tri-layered PEG-based scaffold combined with CS and HA	✓								HA, CS	✓				Highest Col II, low GAG	Compressive modulus: ≈35 kPa	—	—	hBMSCs	—	[191]
											✓			High Col II and GAG	Compressive modulus: ≈65 kPa					
												✓		Highest GAG and Col X	Compressive modulus: ≈75 kPa					
Multi-layered scaffold based on Col I and HA	✓	Tubular porosities							Collagen, HA, HAp	✓				-	Compressive modulus: ≈7.2 KPa	High fibrillar collagen anisotropy	—	—	—	[193]
											✓			-	Compressive modulus: ≈12.7 KPa	Lowest fibrillar collagen anisotropy				
													✓	-	Compressive modulus: ≈13.9 KPa	High fibrillar collagen anisotropy				
Decellularized cartilage ECM		Tubular porosities, nanofibrous pattern							AC ECM			✓		High Col II and GAG	—	Aligned vertical nanofibrillar structure with cell orientation along the microtubules	Ellipsoidal and spindle shape MSCs	Rabbit MSCs	Subcutaneous implantation in the dorsa of nude mice	[194]
Bilayered scaffold based on Gelatin, ALG, CS, and HA	✓								β-tricalciumphosphate (TCP), CS, HA	✓				Higher ratio of Col II: Col X, High aggrecan and Col II	Lower stiffness	—	—	3:1 ratio of hMSCS: hACs	Rat osteochondral defect model	[197]
											✓									
												✓								
													✓	High ALPL, Col X, ACAN, Col II, Col I, Higher Col II:Col I ratio, High aggrecan	Higher stiffness			Only hMSCS		

(*Continued*)

Table 1. (Continued).

Biopolymer	Stimuli: Physical cues: Mechanical properties	Stimuli: Physical cues: Morphology/microstructure	Stimuli: External mechanical forces: HP	Stimuli: External mechanical forces: Compression	Stimuli: External mechanical forces: Shear stress	Stimuli: Biological/chemical cues: GFs	Stimuli: Biological/chemical cues: Hormones	Stimuli: Biological/chemical cues: Small molecules	Mimicked zone: ECM	Mimicked zone: Superficial zone	Mimicked zone: Middle zone	Mimicked zone: Deep zone	Mimicked zone: Calcified zone	Obtained mimicked properties: ECM deposition/gene expression	Obtained mimicked properties: Mechanical properties	Obtained mimicked properties: Physical properties	Obtained mimicked properties: Cell morphology and orientation	Obtained mimicked properties: Cell density/type	Obtained mimicked properties: In vivo studies	Ref.
Bilayered scaffold based on ECMs derived from xenogeneic AC and growth plate									AC and growth plate ECMs	✓				Higher sGAG and Col II	—	Collagen network organization (from superficial to deep zones) similar to native condyle upon 12 months scaffold implantation	—	Porcine BMSCs (for in vitro studies)	Goat critically-sized caprine osteochondral defect model	[200]
											✓									
												✓								
													✓	Higher calcium, Col I, Col X, and Vascular endothelial GF (VEGF)						
GelMA/gellan gum HA-based scaffolds									HA	✓				Higher proteoglycan IV	—	—	—	ACPCs of equine cartilage SZ	-	[196]
											✓			Higher GAG and Col II				Equine MSCs		
												✓								
Collagen-based hydrogel									Col II	✓				High GAG, Col II, and PRG4	—	—	—	Rabbit chondrocyte, 4.284×10^7 Cells per mL	—	[162]
											✓			Intermediate GAG, Col II, and PRG4				Rabbit chondrocyte, 2.856×10^7 Cells per mL		
												✓		Low GAG, Col II, and PRG4				Rabbit chondrocyte, 1.428×10^7 Cells per mL		
SPELA-based scaffold	✓	Oriented fibrous patterns				IGF-1, BMP-7			HAp	✓				Highest Col II and SOX-9	Compressive modulus: 80 kPa	Horizontally oriented fibers	—	60×10^6 hMSC Cells per mL	-	[58]
											✓			Highest Col II and aggrecan	Compressive modulus: 2.1 MPa	Randomly organized fibers	—	20×10^6 hMSC Cells per mL		
												✓		Highest Col X and ALP	Compressive modulus: 320 MPa	Perpendicularly oriented fibers	—	15×10^6 hMSC Cells per mL		

(*Continued*)

Table 1. (Continued).

	Stimuli										Mimicked zone			Obtained mimicked properties					
	Physical cues		External mechanical forces			Biological/chemical cues													
Biopolymer	Mechanical properties	Morphology/microstructure	HP	Compression	Shear stress	GFs	Hormones	Small molecules	ECM	Superficial zone	Middle zone	Deep zone	Calcified zone	ECM deposition/gene expression	Mechanical properties	Physical properties	Cell morphology and orientation	Cell density/type	In vivo studies	Ref.
PEG-based hydrogels with norborne and thiol end groups	✓									✓				–	Gradient hydrogels with different stiffness ranged from 2 to 60 kPa to mimic top to bottom layers of cartilage	—	Highest proliferation	Calf chondrocytes	—	[65]
											✓			-			-			
												✓		Highest SOX-9, Col II, and aggrecan Highest GAG/DNA						
													✓	-						
HBC/OCS hydrogel plus MS/CPC paste	✓								CS	✓				Highest SOX-9 and Col II with 20 mg mL^{-1} OCS	Compressive strengths of scaffolds: 1.84 ± 1.05, 3.07 ± 1.16, and 3.69 ± 0.93 kPa	By diffusing HBC/OCS into the porosity of MS/CPC, smooth transition between layers was achieved	—	Rat BMSC	Subcutaneous implantation into the nude mice	[71]
											✓			-						
												✓		Vascularization restrained in this zone with 20 mg mL^{-1} OCS						
Multi-layered collagen-HA- based scaffolds	✓								Collagen, HA, and HAp	✓				High Col II	—	Concentric lamellar pattern was seen in regenerated sub-chondral area at 12 weeks post-surgery, Visible tidemark was seen between cartilage and bone.	Upon in vivo implantation, cells easily infiltrated into the scaffold and adopted zonal phenotype and morphology, round morphology of cells in SZ residing in lacunae was seen and osteon was formed in regenerated bone	Rabbit full-thickness osteochondral defect model		[77]
											✓			-						
												✓		Vascularization						

(*Continued*)

Table 1. (Continued).

Biopolymer	Stimuli: Physical cues: Mechanical properties	Stimuli: Physical cues: Morphology/microstructure	Stimuli: External mechanical forces: HP	Stimuli: External mechanical forces: Compression	Stimuli: External mechanical forces: Shear stress	Stimuli: Biological/chemical cues: GFs	Stimuli: Biological/chemical cues: Hormones	Stimuli: Biological/chemical cues: Small molecules	Stimuli: Biological/chemical cues: ECM	Mimicked zone: Superficial zone	Mimicked zone: Middle zone	Mimicked zone: Deep zone	Mimicked zone: Calcified zone	Obtained mimicked properties: ECM deposition/gene expression	Obtained mimicked properties: Mechanical properties	Obtained mimicked properties: Physical properties	Obtained mimicked properties: Cell morphology and orientation	Obtained mimicked properties: Cell density/type	In vivo studies	Ref.
PVA and Carrageenan-based composite scaffold		Oriented porosities with fibrous structures										✓		Higher GAG and Col II deposition plus better blood vein formation in unidirectional oriented microstructure compared to the porous one	Higher compressive modulus in unidirectional oriented microstructure compared to the porous one	Unidirectional and random porosity	—	Better ATDC5 cell infiltration and more uniform cell distribution in unidirectional oriented microstructure upon in vivo implantation	Subcutaneous rat model	[80]
PCL-based scaffolds		Oriented fibers								✓				-	—	Aligned electrospun fibers	—	MSC	—	[84]
											✓					Random electrospun fibers				
												✓				Cryo-printed fibers in the form of helix				
PCL-based scaffolds		Oriented micro/nano fibers								✓				Higher GAG and Col II level on nanofibrous structure, downregulation of GAG on microfibrous		Aligned PCL fibers (fiber diameters: 500 and 3000 nm) with oriented cells along the fibers	Elongated cells	hMSCs	—	[96]
PCL, PLA, and PGA-based layers coated with CS	✓	Nanopatterned surfaces: Pillars and gratings							CS	✓				PRG4 expressed on softer nanogratings	Surface compression modulus of nanopillar were 149.3, 82.6, and 25.6 MPa while for nanograting were 161.6, 88.1, and 29.9 MPa for PGA, PLA, and PCL, respectively	—	From rounded to polygonal MSCs when stiffness of nanopillars increased and elongated on nanogratings	MSCs	—	[99]
											✓			Col II, Col 9, and CILP were expressed better on nanopillars, specifically on soft and medium stiffness						
												✓								

(*Continued*)

Table 1. (Continued).

	Stimuli										Mimicked zone			Obtained mimicked properties						
	Physical cues			External mechanical forces			Biological/chemical cues													
Biopolymer	Mechanical properties	Morphology/microstructure	HP	Compression	Shear stress	GFs	Hormones	Small molecules	ECM	Superficial zone	Middle zone	Deep zone	Calcified zone	ECM deposition/gene expression	Mechanical properties	Physical properties	Cell morphology and orientation	Cell density/type	In vivo studies	Ref.
PCL films coated with CS		Spatially controlled nano patterns; nanoholes, nanopil-lars, and nanogrills							CS	✓				PRG4, while Col I was also expressed on nanogrills	≈30 MPa surface stiffness (Nanogrills)	Nano-grills simulated the parallel SZ and DZ collagen fibers; nano-holes mimicked the pores formed among the randomly organized collagen fibers; and nano-pillars emulated intersecting point of the randomly oriented collagen fibers	Spindle-shape MSCs on nanogrills	hMSCs	—	[100]
											✓			Col II and aggrecan, while Col X was also expressed on nanopillars	≈40 and ≈25 MPa surface stiffness for Nanoholes and nanopillars, respectively		Polygonal MSCs on nanoholes			
												✓		-	≈30 MPa surface stiffness (Nanogrills)		Rounded MSCs with filopodial extrusion on nanopillars			
Silk mesh with chitosan hydrogel		Nano pillars and fi-brous/mesh structure						KGN		✓				High expression of Col II, SOX-9 and aggrecan	Silk compressive modulus: 921 MPa representing SZ and chitosan hydrogel shear modulus: 10.2 kPa representing synovial fluid	Hydrophilic surface by N implantation, aligned expressed Col II fibers parallel to the surface, Silk mesh with microfibers also mimicked SZ collagen fibers	Flattened ellipsoidal hAMSCs shape on nanopillars	Aligned hAMSCs organized along the expressed collagen fibers parallel to the surface	—	[23]
Silk fibroin, gelatine, CS, and HA- based scaffolds				✓					CS, HA			✓		High expression of Col X and aggrecan, no difference in Col I and Col II level	Compressive modulus: around 110 and 80 kPa after seeding chondrocytes and BMSCs, respectively	—	—	Human chondrocytes and MSCs	—	[135]

(*Continued*)

Table 1. (Continued).

	Stimuli										Mimicked zone			Obtained mimicked properties						
	Physical cues			External mechanical forces		Biological/chemical cues														
Biopolymer	Mechanical properties	Morphology/microstructure	HP	Compression	Shear stress	GFs	Hormones	Small molecules	ECM	Superficial zone	Middle zone	Deep zone	Calcified zone	ECM deposition/gene expression	Mechanical properties	Physical properties	Cell morphology and orientation	Cell density/type	In vivo studies	Ref.
Scaffolds based on silk and chitosan		Gradient porosities		✓					HAp	✓				Compression enhanced Col II and aggrecan while SOX-9 was expressed more in perfusion group	Highest compressive stresses achieved after 2 weeks of compression loading (≈26 kPa)	Porosity diameter 332.71 ± 52.63 µm	—	Rat BMSCs for in vitro studies	Unilateral arthrotomy on knee joint of mini-pig	[136]
											✓					Porosity diameter 287.31 ± 47.13 µm				
												✓				Porosity diameter 266.12 ± 66.74 µm				
													✓			Porosity diameter 159.70 ± 58.51 µm				
Chitosan thermogel	✓							KGN		✓				High expression of Col II, aggrecan, and SOX-9	Shear modulus:78 ± 5 kPa	Tunable physio-mechanical properties such as shear modulus, swelling, gelation time/temperature	—	hAMSCs	—	[22]
											✓									
PCL-GelMA scaffold		Oriented fibrillar structure		✓						✓				High Col II and lubricin	Scaffold equilibrium modulus: ≈3.5 MPa	Parallel oriented collagen fibers to the top surface	—	Mixture of BMSCs and chondrocytes (3:1)	—	[137]
											✓			High sGAG		Random orientation of collagen fibers		BMSCs and chondrocytes		
												✓		High calcium deposition and Col X		surface orientation of collagen fibers		BMSCs		
Agarose hydrogel				✓		TGF-β3				✓				High Col II and PRG4 secretion with low sGAG	Dynamic modulus: ≈1.45 MPa.	—	—	Porcine infrapatellar fat pad-derived stem cells (FPSCs)	—	[140]
Fibrin-HA hydrogel				✓	✓					✓				High expression of collagen and GAG	Young's modulus 93.15 kPa	Close-packed and horizontally oriented collagen fibers	—	Pig chondrocytes	—	[151]
											✓			–	—	—				
												✓				Less concentration of collagen fibers with more isotropic orientation	Vertical arrangement of cells			

(*Continued*)

Table 1. (Continued).

Biopolymer	Stimuli: Physical cues: Mechanical properties	Stimuli: Physical cues: Morphology/microstructure	Stimuli: External mechanical forces: HP	Stimuli: External mechanical forces: Compression	Stimuli: External mechanical forces: Shear stress	Stimuli: Biological/chemical cues: GFs	Stimuli: Biological/chemical cues: Hormones	Stimuli: Biological/chemical cues: Small molecules	Stimuli: Biological/chemical cues: ECM	Mimicked zone: Superficial zone	Mimicked zone: Middle zone	Mimicked zone: Deep zone	Mimicked zone: Calcified zone	Obtained mimicked properties: ECM deposition/gene expression	Obtained mimicked properties: Mechanical properties	Obtained mimicked properties: Physical properties	Obtained mimicked properties: Cell morphology and orientation	Obtained mimicked properties: Cell density/type	Obtained mimicked properties: In vivo studies	Ref.
Cell-derived ECM (neo-cartilage construct)					✓	TGF β1, LOXL 2			Cell-derived ECM	✓				High collagen, PKD1 and PKD2 expression	Under FIS, aggregate modulus, shear modulus, UTS, and Young's modulus of human neocartilage constructs reached to ≈60 kPa, 30 kPa, 1 MPa and 2 MPa, respectively	High collagen fibers crosslinking density upon applying shear stress	—	Juvenile bovine and human chondrocytes for in vitro studies and bovine chondrocytes for in vivo studies	Subcutaneous implantation on athymic mice	[161]
											✓									
												✓								
HA-based multilayer scaffolds with PLA nanofiber meshes		Oriented fibrillar patterns							HA	✓				Low GAG and Col II, high Col I	Compressive modulus: 15.47 + 3.5 kPa	Aligned horizontal fibers	Aligned elongated cells	Primary bovine chondrocytes	—	[192]
											✓			Intermediate GAG and Col I and high Col II	Compressive modulus: 16.16 + 2.9 kPa	Randomly oriented fibers	Randomly oriented aggregated cells			
												✓		Highest GAG, lowest Col I	Compressive modulus: 15.85 + 4.2 kPa	Vertical channels	Columnar oriented cells			
Chitosan-based injectable nanocomposite thermogel	✓							KGN			✓			High expression of Col II, aggrecan and SOX-9	Shear modulus:167 ± 5 kPa	Tunable physio-mechanical properties such as shear modulus, swelling, gelation time/temperature	—	hAMSCs	—	[180]
GMP-PCL electro-spined fiber with GelMa hydrogel		Interwoven fibers with different porosity sizes and fibrillar dimension		✓		TGF-β1				✓				Increase GAG depth wise	Similar stress-relaxation behavior to native cartilage	Fibers with 0–45–90–135°, 50 µm interfiber distance, ≈70% porosity, 10% of the whole structure height	—	Equine chondrocytes	—	[83]
											✓					Fibers with 0–90°, 800 µm interfiber distance, ≈97% porosity, 90% of the whole structure height				
												✓								

(*Continued*)

Table 1. (Continued).

Biopolymer	Stimuli										Mimicked zone				Obtained mimicked properties						
	Physical cues			External mechanical forces			Biological/chemical cues														
	Mechanical properties	Morphology/microstructure	HP	Compression	Shear stress	GFs	Hormones	Small molecules	ECM	Superficial zone	Middle zone	Deep zone	Calcified zone	ECM deposition/gene expression	Mechanical properties	Physical properties	Cell morphology and orientation	Cell density/type	In vivo studies	Ref.
GelMA/CSMA		Micro ribbon morphology							CS	✓				Highest and lowest amount of Collagen and sGAG, respectively	≈55 kPa	GelMA:CSMA (100:0) Aligned micro ribbon	—	MSC	—	[90]
											✓			–	≈225 kPa	GelMA:CSMA (90:10)				
												✓		Lowest and highest amount of Collagen and sGAG, respectively	≈452 kPa (in the range of native articular cartilage)	GelMA:CSMA (75:25)				
PCL/methacrylated alginate		Fiber orientation with variable filament gap								✓				Highest Col II/Col I ratio	Highest tensile and compressive modulus, 61.57 ± 2.05 MPa and 20.44 ± 1.32 MPa, respectively	Orthogonal design with 0/90° lay-down pattern and 300 µm filament gap		Rat BMSCs	—	[87]
											✓			Highest Col I and Col X		0/60° lay-down pattern and 500 µm filament gap				
												✓		Highest Aggrecan and SOX-9		0/30° lay-down pattern and 700 µm				
Agarose					✓					✓				Higher secretion of Col II, PGs, and PRG4 No change in Col I	—	Parallel collagen Fibers to the surface	Flattened chondrocytes	40×10^6 cells per mL	—	[157]
Fibrin					✓					✓				Narrow PRG4 distribution	—	Comparable thickness with native tissue	—	Minipig chondrocytes (10^7 cells per mL)	Porcine knee chondral defect model	[156]
											✓			Higher Col II and Col 9		Distinctive zonal separation	Similar columnar arrangement			
												✓								

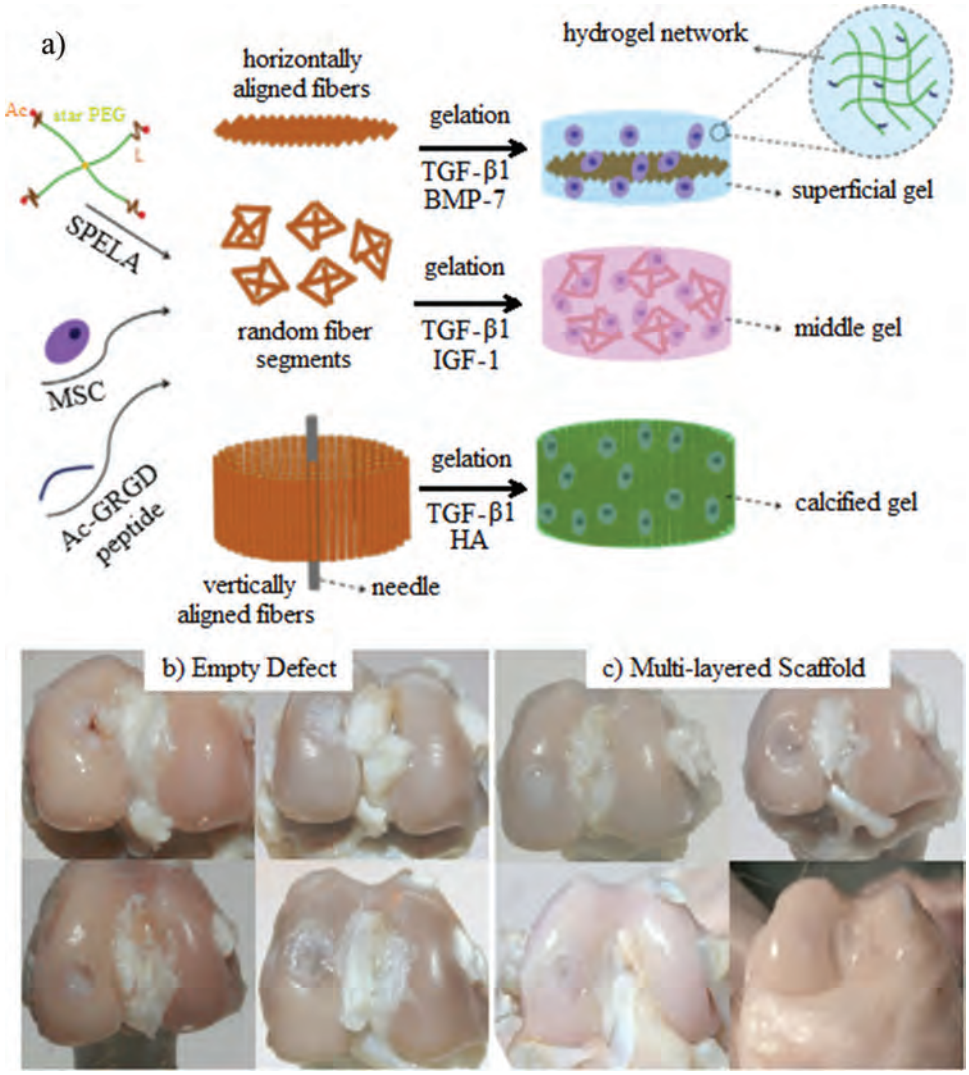

Figure 3. a) Schematic representation of the construct made of the SPELA hydrogel with different mechanical properties and incorporation of collagen fibers with the preferential directions and specific GFs corresponding to each zone of the cartilage for zonal cartilage TE. Reproduced with permission.[58] Copyright 2016, Elsevier. Visualization of microscopic repair of the distal femur defects at 12 weeks post implantation: b) Empty defect group and c) Multi-layered scaffold group. Reproduced with permission.[77] Copyright 2016, Elsevier.

higher chondrogenic properties.[54–57] Hydrogels based on the star acrylate-terminated lactide-chain-extended polyethylene glycol macromer (SPELA) with different stiffness have been fabricated to mimic the three different cartilage zones.[58] The matrix compressive moduli of 80 kPa, 2.1 MPa, and 320 MPa are chosen for the SZ, MZ, and CZ, respectively (**Figure 3**a). Meanwhile, to better mimic the native cartilage ECM, poly(D,L-lactide) (PLA) nanofibers are dispersed in the hydrogels horizontally, randomly, and perpendicular to the surface of the SZ, MZ, and CZ, respectively. Parallel dispersion of PLA nanofibers results in significantly higher expression of Col II in the SZ. Although specific GFs are used for each zone, the matrix physico–mechanical properties exhibit more dominant effects in modulating the cell fate than biological stimuli. For example, the SZP expression is higher in the superficial than calcified gels, although transforming growth factor β1 (TGF-β1) is supplemented in both.[58]

Considering the stepwise cartilage gradient characteristics, it is highly desirable to design scaffolds with the temporal morphology and mechanical properties while avoiding sharp zonal interfaces.[59–64] This offers a tissue scalable cell niche for zonal differentiation of Mesenchymal stem cells (MSCs) as demonstrated by Zhu et al.[65] For example, gradient photo-responsive polyethylene glycol (PEG) hydrogels have been developed by adjusting the hydrogel concentration. The graded hydrogel possesses five regions based on the stiffness ranging from 2 to 60 kPa corresponding to the SZ to DZ. MSCs cultured in each region secrete different biomarkers comparable to the natural cartilage zonal configuration probably due to the sensed stiffness. Although the tissue-scale hydrogel does not show a sharp zonal interface, but future improvement of the mechanical properties and tuning the cell density similar to the native cartilage may add value to the structure.[66–68]

In addition to the target tissue/zone mechanical properties, the stiffness of biomaterials should be adjusted according to the cell type.[69] For instance, although MSCs proliferate and regenerate cartilages better on the gradient PEG-based hydrogel with relatively soft stiffness (1–15 kPa), juvenile chondrocytes perform better on stiffer hydrogels (stiffness: 15–50 kPa). MSCs on the softest hydrogel (stiffness:1 kPa) increase the compressive modulus by about 30 times due to extensive ECM deposition after culturing for 3 weeks. In contrast, the amounts of newly formed sGAG and Col II by chondrocytes increase on the stiffer substrate. Subcutaneous implantation of the MSCs-seeded platforms in immune-deficient mice show promoted angiogenesis by MSCs after 2 weeks with secretion of collagen type-X (Col X), implying that the cartilage is going to be replaced by bones and the cells undergo endochondral ossification. However, chondrocytes seeded on stiff scaffolds do not develop considerable Col X or blood vessels which keep the original cartilage phenotype.[69]

Furthermore, gradient of mechanical properties is combined with gradient of biochemical components like chondroitin sulfate (CS) to show better chondroinductive results. Although, this strategy led to similar chondrocytes morphology and sGAG distribution to the native cartilage and higher collagen deposition, however, low Col II/Col I ratio in the SZ and high expression of MMP13 gene as a hypertrophy marker necessitate a better strategy to tackle such drawbacks.[70]

Although the above studies point out the importance of adjusting niche signals based on the cell type and mechanical properties of the scaffold, cell-seeded hydrogels have not been assessed using a relevant animal model to examine the functionality of the construct in the real tissue environment by taking into account hypoxia, avascular, and acellular nature of the cartilage while being exposed to different types of mechanical forces during the healing process.

3D printing of cartilaginous structures with zonal configurations fosters the development of personalized engineered scaffolds.[71–73] For example, the combination of calcium phosphate cement (CPC) with mesoporous silica (MS) has been 3D-printed according to the shape of the patient's injured site. The hydrogel based on hydroxybutyl chitosan (HBC) crosslinked with oxidized CS (OCS) is 3D-printed on top and the in vivo results after subcutaneous implantation of the scaffolds into the dorsal region of nude mice show that MS/CPC promotes angiogenesis and subchondral bone development. Increasing the gel OCS concentration triggers strong anti-angiogenesis effects, while the MSCs remain spherical and express chondrogenic markers including SOX-9 and Col II. Therefore, the top layer promotes the hyaline cartilage because of the proper physical, biological, and anti-angiogenesis properties, whereas the bottom one stimulates subchondral bone. Owing to diffusion of the HBC/OCS hydrogel through pores, a transition layer is also formed.[71] Although the feasibility of this approach to fabricate a 3D structure with a similar defect shape is demonstrated, the scaffold performance requires further investigation using a clinically relevant animal model besides subcutaneous implantation.

On top of the current available cell-based therapies, there is a huge clinical demand for user friendly and off-the-shelf solutions. In this regard, a multi-layer scaffold based on collagen and HAp has been designed to mimic the three layers of AC.[74–76] Combination of Col I, II, and HA for the SZ, Col I, II, and HAp for the intermediate layer, and Col I and HAp for the DZ have been implemented for zonal cartilage regeneration.[77] According to the International Cartilage Repair Society (ICRS) assessment, the healed critical-size defects in rabbit knee by the multi-layer scaffold obtains a higher score than empty defects, as it is analogous to the adjacent host tissues compared to the fibrous and discontinuous ones generated from empty defects (Figure 3b,c). This scaffold confines bone regeneration and vascularization underneath the cartilage tidemark to avoid early degenerative damage.[77–79] Besides the dense subchondral tissue development, the cartilage nature of the other parts is preserved, particularly compared with the fibrous tissues generated from empty defects with the subchondral cyst and deep fissure. Although this scaffold is cell-free at the time of implantation, the host cells can easily infiltrate and differentiate into the desired cell types under the influence of zonal configurations and their specific mechanical and physical properties.[77]

3.1.2. Morphology, Microstructure, and Surface Topography of Biopolymers

The well-known physical parameters such as surface nanofeatures and scaffold morphology and microstructure should be optimized based on the stepwise cartilage heterogeneity which is a key point of effective cartilage regeneration. In this regard, morphologies that simulate the collagen orientation/organization in cartilaginous zones have been developed. For example, scaffolds with mesh/fibrillar patterns could mimic collagen fibrillar morphologies with different orientations in cartilage layers. Such morphologies can be developed in polymeric scaffolds by introducing unidirectional/tubular porosities through different material processing methods including but not limited to the unidirectional freezing or electrospinning approach.[80–82]

A bizonal scaffold is made by electrospinning of GMP-polycaprolactone (PCL) with different porosity dimensions and fibers alignment for superficial, middle/deep zones which exhibits similar stress-relaxation to the native cartilage tissue although its equilibrium modulus is not similar.[83] Electrospun structures representing SZ and MZ made from PCL, are mounted on top of a helix-shaped cryo-printed PCL scaffold to mimic the complexity of AC. Although the reduced Col I expression along with the elevated aggrecan expression upon culture represent the cartilage maturation, however the study of their spatial distribution could be clarified for better understating.[84] Zone-dependent microstructures in layered scaffolds such as oriented fibrous or homogeneous pores[85–88] can result in diverse cellular phenotypes.[78,80,89] It is shown that, micro-ribbon morphology of gelatin methacrylate (GelMA) and (CS methacrylate) CSMA presents superior properties in terms of zonal-biomarkers expression and mechanical properties compared to the traditional hydrogel format.[90] Different combinations of GelMA and CSMA are chosen for SZ, MZ, and DZ, based on the reduction effect of CS content on collagen expression, and the highest compressive modulus that can be achieved. Besides this, by introducing aligned micro-ribbons to the surface for mimicking SZ, expression patterns of collagen and sGAG appear to be more similar to that of the natural cartilage layers. Furthermore, this structure shows its superiority against the traditional one by provid-

ing 452 kPa compressive modulus in the DZ, while withstanding more than 100 kPa before failure. Aside from the lack of in vivo studies, expression of other genes should be implemented. Additionally, the limited expression of Col X in all layers along with poor mechanical properties of SZ and DZ should be addressed in the next studies.

Zhang et al.[80] have fabricated a polyvinyl alcohol (PVA)-carrageenan-based construct by unidirectional freezing followed by lyophilization to produce oriented porosity. In vivo results show that in addition to vascularization in the scaffold, the unidirectional porosity provides the suitable mechanical support (≈6 MPa compressive stress at 55% strain before immersing in PBS) and space for cells to infiltrate and secrete Col II and sGAG. By considering vascularization, the construct can mimic the cartilage DZ. Polymer chain modification is another way to adjust the pore sizes and improve the mechanical properties in thermoresponsive hydrogels.[91] Accordingly, better interconnectivity and larger pore size are achieved by introducing phenylalanine into PA-PEG-PA co-polymer, which result in significantly better chondro-inductive behavior in vivo. Nevertheless, the mechanical properties of the newly formed tissues are weaker than the native cartilage and there is still room for improvement.[92] Also, PLGA-PEG-PLGA thermogel made by co-polymerization of PLGA and PEG, is incorporated with BMSCs by which a full-thickness cartilage is successfully regenerated, providing 80% of the native cartilage Young's modulus.[93] The regenerated tissue by the co-polymerization approach has higher ICRS score with higher GAGs and Col II expression compared to the non-cell loaded gel.[92–94]

Yang et al.[95] have fabricated fibrous and porous hydrogels based on methacrylated Col I. The bone marrow MSCS (BMSCs) seeded on the fibrous structures upregulate the expressions of Col II, SOX-9, and sGAG, while Col X is also expressed more compared to the porous structure. The in vitro and in vivo evidence suggests that the fibrous pattern enhances the chondrogenic properties better than the porous structure, but still not able to inhibit MSCs hypertrophy. In the in vivo experiments, the scaffolds are implanted subcutaneously in nude mice, but evaluation using other common animal models for cartilage repair is required to confirm similar gene expressions by MSCs after introducing them to the joint/cartilage.

In another experiment,[96] PCL is electrospun with two different fiber diameters (500 and 3000 nm) to mimic the SZ. Although MSCs proliferation is improved by culturing on the nanofibrous network and SZ relative biomarkers are expressed, the cells elongate and contradict the flattened/ellipsoidal chondrocytes in the natural cartilage SZ.[97]

The importance of a guided microstructure for cartilage zonal tissue differentiation has been demonstrated by Camarero–Espinosa et al.[98] A multi-layer PLA nanocomposite is developed with the microarchitecture, mechanical properties, and chemical cues mimicking the mature AC. To emulate the ECM environment and tune the cells phenotype, chemical cues are introduced in the form of rod-shape cellulose nanocrystals (CNCs) containing a few sulfate (S-CNCs) or phosphate (P-CNCs) ester groups by which the mechanical properties can be improved. The thermally induced phase separation (TIPS) approach is applied to create tubular pores parallel to the surface for the superficial layer and guide ECM deposition along them. The middle layer is produced with S-CNCs/PLA that produces the spherical chondrocyte morphology accompanied by disordered ECM, suggesting that S-CNCs can have a high concentration of sGAGs to dominate the disorganized ECM morphology. Furthermore, orthogonally oriented tubular pores on the surface of the P-CNCs/PLA layer replicate the collagen arrangement in the deep CZ (**Figure 4**a,b). The phosphate groups on the nanoparticle surface promote HAp formation and the graded chemical cues and pore size in the final construct lead to depth-dependent mineralization. Despite achieving similar H_a values reported for AC (0.1–2 MPa), the weak E is compensated by the ECM deposited by the cells after culturing for 4 weeks (0.16 ± 0.06 MPa), but it is still lower than that of the native cartilage (0.3–0.8 MPa).[98]

Surface topographies on the other hand substantially affect the cell morphology and differentiation. Hence, they can be employed as effective regulators of cell fate/phenotype according to our needs. The roles of stiffness and surface topography on chondrocytes differentiation, shape, and proliferation have been studied by Wu et al.[99] using PCL, PLA, and polyglycolide (PGA) with different stiffness and two surface topographies; nanopillars and nanogratings. The morphology of MSCs changes from round to polygonal when the stiffness of the nanopillar substrate increases. Meanwhile, the fibroblastic cells on the nanogratings are elongated with increased cell fiber lengths when the stiffness is raised. The nanopillars express the MZ and DZ biomarkers such as Col II, cartilage intermediate layer protein (CILP), COMP, and Col IX compared to the nanogratings, especially on soft and medium stiffness substrates. On the other hand, PRG4 is mainly expressed on the nanogratings.[99] Similarly, the effects of PCL-based nanopillars, nanoholes, and nanogrills on the cell morphology, differentiation, and proliferation of human MSCs (hMSCs) have been investigated.[100] A round morphology with filopodial extrusion, polygonal, and spindle shape are observed from nanopillars, nanoholes, and nanogrills, respectively. The nanogrills elevate both the SZ and fibrocartilage formation due to larger expressed amounts of PRG4 and Col I, respectively. Meanwhile, the cells on the nanopillars express Col II and aggrecan (biomarkers related to the hyaline cartilage) and Col X with insignificant amount of PRG4.

Although the aforementioned studies specify the importance of the biomaterials mechanical and physical properties in achieving zonal cartilage configuration, consistency of the chondrocytes shape and expressed zonal biomarkers on specific nanopatterns is challenging. Dehghan–Baniani et al.[23] have employed hexagonally close-packed arrays of silk nanopillars fabricated by colloidal lithography and oxygen plasma etching to emulate the SZ. A chondro-inductive small biomolecule, kartogenin (KGN), is conjugated with the nanopillars to promote chondrogenesis of human adipose MSCs (hAMSCs). A chitosan hydrogel is combined with the substrate to deliver the viscoelastic properties resembling those of the synovial fluid. The nanopillars alter the hAMSCs morphology from being elongated to nearly flattened ellipsoidal to mimic the chondrocytes in the SZ (Figure 4c–g). Secretion of Col II, SOX-9, and aggrecan is elevated due to the nanopatterns and gradual KGN release. The substrate elastic modulus is about 920 MPa but as the pillar bending rigidity is much lower, MSCs can bend it and form the ellipsoidal morphology mimicking the SZ chondrocytes.[99,101–104] Col II expressed by the cells is also oriented parallel to the surface similar to the innate SZ

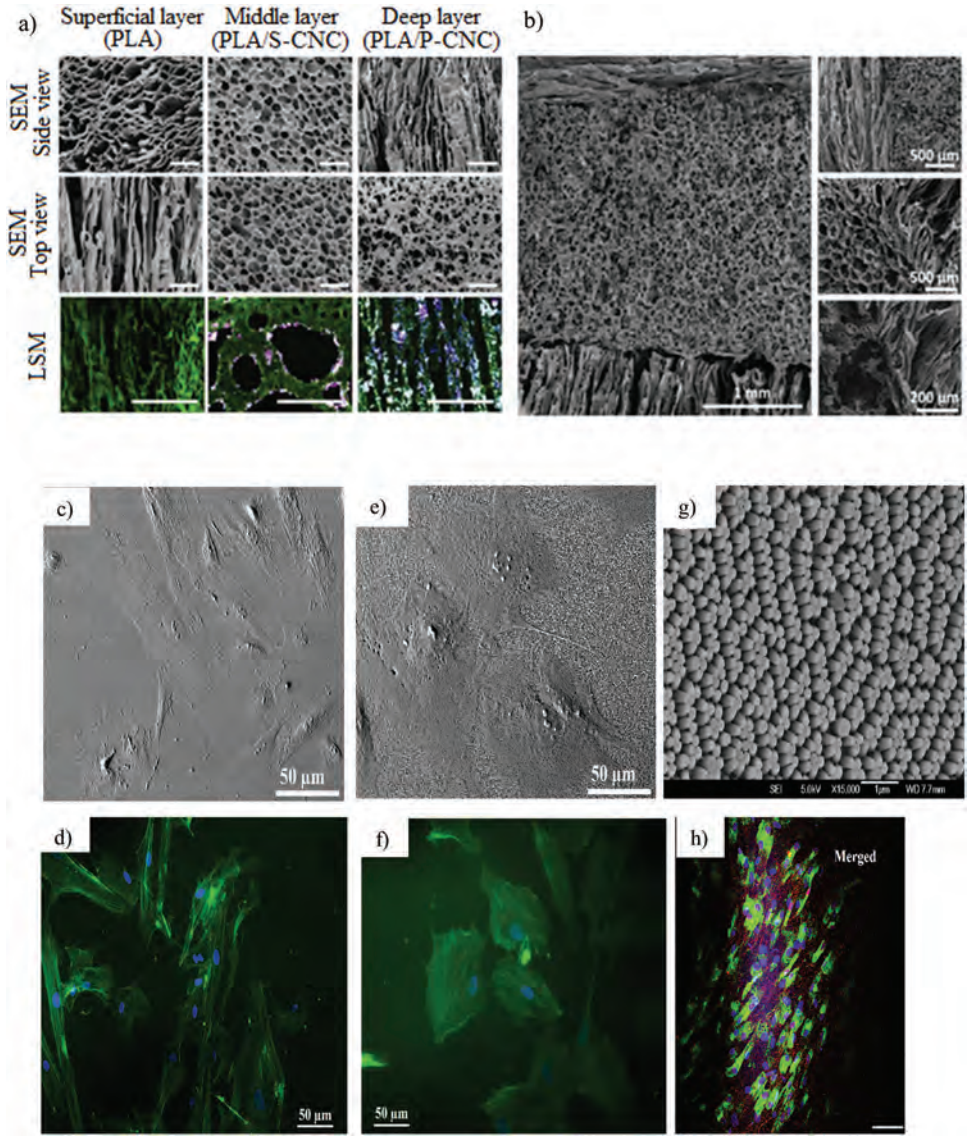

Figure 4. a) SEM images of the different layers from the top and side view and laser scanning microscopy (LSM) images revealing the location of Rhodamine-labeled fluorescent CNCs (pink) and Alexa 488-labeled PLA (green) in the different layers (Scale bars: 200 µm). b) SEM images of different layers after assembly showing pore shapes and sizes. Reproduced with permission.[98] Copyright 2016, Elsevier. SEM and cytoskeleton staining of hAMSCs cultured on c,d) N implanted silk loaded with KGN and e,f) N implanted nanopillar silk loaded with KGN, showing how nanofeatures manipulate the cell morphology. g) SEM image of silk nanopillars. h) Immunoflourescent staining of expressed Col II (green) which are oriented parallel to the surface and SOX-9 (red) on N implanted nanopillar silk loaded with KGN (Scale bar: 100 µm). Reproduced with permission.[23] Copyright 2021, Wiley-VCH GmbH.

(Figure 4h). Previous studies have shown that the SZ biomarkers express mostly on the nanogratings or nanogrooves, but the cell morphology is not completely consistent with the original state in healthy tissues. Nevertheless, evaluating the SZP expression and wear resistance properties in conjunction with in vivo tests imparts more information about the application of this platform.[23]

The SZ fibrillar collagen and mechanics are mimicked by PCL Fibers laminated to a PCL scaffold wherein NaCl porogen is employed to adjust the desired porosity for deep cellular infiltration and substantial ECM deposition.[105] Considering the increasing trend of sGAG/DNA in the bulk scaffold, a more DZ-resembling construct is likely to be developed upon extended culturing. The reduced roughness of the first layer retains the frictionless properties of the articulating surface and the aligned Fibers provide similar topographical cues and tensile strength of the SZ. The depth-dependent expression of SZP along with the zone-specific morphology of chondrocytes needs to be emulated.[105]

In another attempt inspired by zone-dependent collagen fiber architecture in AC, a tri-layered stratified PCL composite is 3D-printed and seeded with rBMSCs followed by impregnation with the cell-loaded methacrylated alginate (ALG) hydrogel. The interconnected pores with gradient geometries along the longitudinal direction offer a conducive microenvironment to regenerate cartilages and emulate the SZ, MZ, and DZ.[87] Although the

compressive moduli of the three zones resemble those of the natural cartilage (2.75–21.4 MPa), tuning the fiber diameters and expression of zone-specific markers throughout the composite can improve the properties.[87] Girão et al.[88] have imitated the anisotropic fibrillar collagen arrangement in the SZ, MZ, and DZ by intercalating PCL fibers in the graphene oxide–collagen hydrogel which assembles the fibrous layers with a microporous network. The DZ resists more to compression (compressive modulus: ≈136.77 KPa) than the other layers because of the vertically orientated fibers. Despite the depth-dependent mechanical and morphological properties, the biological properties must be investigated both in vitro and in vivo.[88]

Despite multi-layered structure can impact zonal cartilage development, discrepancy also reported that star-PEG hydrogels combined with PCL meshes with both zonal and non-zonal intentions result in worse healing conditions after implantation for 6 months in mini-pigs.[106] Dislodging of the hydrogel containing cells and the PCL leading to bone loss, lower PG expression, and higher formation of cysts and fibrous cartilage, which are the main reasons for the poor outcome. Empty defects are healed better while there is no significant difference between the zonal and non-zonal constructs. These studies[106,107] indicate that while some zonal/non-zonal constructs show promising results in vitro or even for a short period in vivo experiments, more work is needed prior to their clinical practice and routine approaches such as microfracture are still the first and best option for surgery operations.

3.2. External Mechanical Forces

External forces have undeniable effects on cell fate and can be opted to develop zonal cartilage.[108] Among them, mechanical cues are one of the most interactable forces with cartilage tissue in daily activities. They stimulate the cells in the two ways of active and passive forms. While the passive form originates from the basic properties of biomaterials, the active form is mainly derived from extrinsic mechanical force/deformation imposed to the cells which boosts ECM deposition.[109,110] Hyaline cartilage repeatedly experiences mechanical force during normal life.[111] The dynamic force alters the cell microenvironment and subsequently the intracellular forces and cellular response.[112,113] The cells interact with ECM molecules via membrane proteins including adhered molecules and integrins, cytoskeleton constituents, and perturbation of ion channels. These are crucial mechanotransduction pathways by which cells sense and transfer the mechanical stimuli.[114] Therefore, the hydrostatic pressure (HP), fluid shear force, and compression can be employed as external stimuli to achieve better cartilage regeneration.[115]

3.2.1. Hydrostatic Pressure

The cartilage is a biphasic entity composed of liquid and solid compartments and continuously subjected to dynamic pressure. The interstitial fluid applies a constant HP to the solid phase. The hydrostatic signal is transferred through mechanosensitive ion channels such as the transient receptor potential family (TRP) like TRPV1, TRPV4, TRPC1, and piezo ion channel family including PEIZO1.[116–118] Consequently, applying HP in cellular or animal models is believed to create a more realistic experimental condition through effect on protein secretion and cell phenotypes.[119–122] Applied HP along with other external forces elevates secretion of Col II, SOX-9, sGAG, Collagen/DNA, and GAG/DNA while suppressing Col I and Col X.[123–126] Absence of HP may upregulate osteoarthritis genes such as that observed during long-term space mission and other more common unloading conditions in bedridden patients.[127–130]

Some reports have revealed the advantages of HP for chondrogenicity compared to other mechanical stimuli[131–133] and the importance of substrate stiffness and timing of mechanical stimulation on the chondrogenic results has been disclosed.[134] Although these studies indicate the effectiveness of HP on chondrogenicity and upregulation of hyaline cartilage, in the last decade, published work on zonal configuration of cartilage tissue was not found in our research. This may stem from the difficulty in applying different mechanical forces to different scaffold layers, specifically where the layer dimensions are small.

A collagen-I based matrix (NeoCart) has been seeded with chondrocytes and incubated for 6 weeks in a bioreactor. After exposure to HP[12] at a low pressure in knee-like environment, better results are observed compared to microfracture.[9,10] The commercial product is still under investigation for clinical trial phase III,[11] but nonetheless, it shows the great potential of external mechanical stimuli to improve cartilage TE. However, even these biomaterials are not suitable for advanced osteoarthritis injuries and therefore, a meticulously designed platform is highly desirable. Up to now, most of the works have been done in vitro and there is a lack of suitable in vivo studies. Furthermore, most of them were focused on upregulation of general hyaline cartilage biomarkers regardless of the spatial distribution or zonal specificity and there is less sign of the accurate zonal cartilage TE.

3.2.2. Compression

Since compressive forces are routinely applied to human joints, numerous attempts have been made to simulate the conditions when developing cartilage constructs. For instance, applying compression regime while the construct is immersed in PBS, can mimic the real conditions and result in higher GAG and Col II production.[83] The level of secreted GAG in this condition is similar to the one with presence of TGF-β1 in the static mode. Nevertheless, sole compression may not be sufficient to fully restore cartilages with the zonal organization.[85]

Sawatjui et al.[135] have utilized dynamic compressive force as the mechanical stimulus to BMSCs and chondrocytes seeded on silk fibroin scaffolds to develop a cartilaginous construct. Although more aggrecan and GAG/DNA are expressed by the cells subjected to compression than the control group, there is no difference in the Col II/Col I ratio. Specific targeted zones are not mentioned and by taking upregulation of Col X into account, the platform is beneficial to the cartilage DZ.[135]

In another experiment,[136] a four-layer scaffold made from chitosan, silk fibroin and nano-HAp has been designed to mimic the SZ, MZ, DZ, and CZ. rBMSCs are cultured on the layers and the platform is subjected to on/off cyclic compression loading (at 10% strain and 0.5 Hz, 2 h each time/4 h off, 4 times a day plus continuous perfusion (10 mL min^{-1})) for 2 weeks in vitro. After-

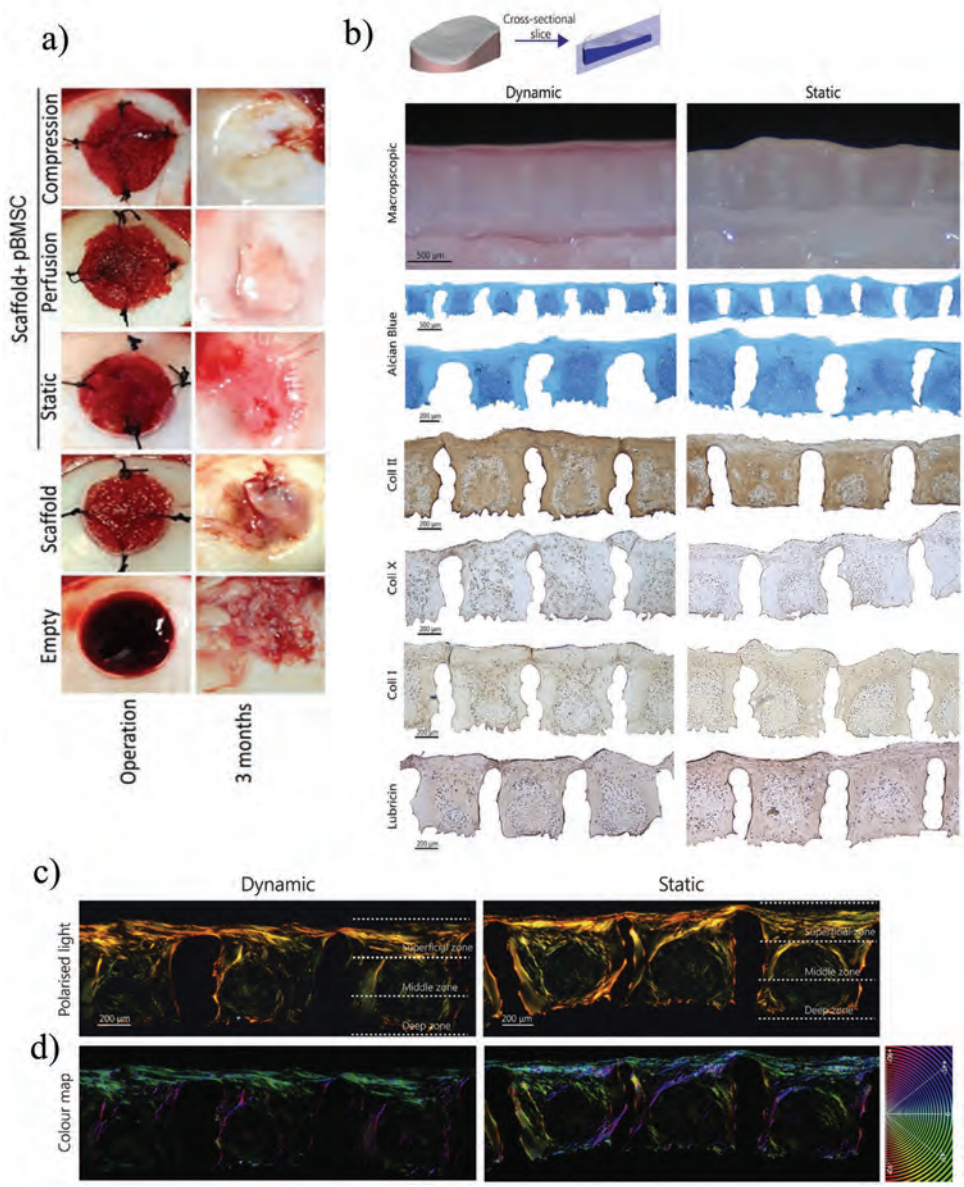

Figure 5. a) Digital image of the injured site on the day of operation and 3 months later. Visible cyst and fibrous cartilage can be seen from all the groups except the compression one, wherein native-like cartilage fills the defect. Reproduced with permission.[136] Copyright 2019, Wiley Periodicals LLC. b) Schematic and macroscopic cross-sectional view of the cell-seeded 3D printed PCL structure with a new cartilage layer formed on top by Alcian blue, Col II, Col X, Col I, and lubricin staining. c) Polarized light and d) Color maps showing the collagen fiber orientation after in vitro cell culturing for 10 weeks. Reproduced with permission.[137] Copyright 2019, Elsevier.

ward, the cell-seeded scaffold is implanted into a mini-pig joint cartilage defect. The bottom layer is made of chitosan/nano-HAp and the other three layers are fabricated using a gradient composition of chitosan and silk fibroin in the reverse order. The in vivo results indicate that the mechanical loading regime generates new tissues with a similar appearance as the native AC without detectable fibro cartilage (**Figure 5**a).[136]

By 3D-printing a PCL microchamber, human tissue-scaled scaffolds are made to promote full cartilage development from the SZ to the endochondral region under dynamic (0.05 mm s^{-1}) and static culturing conditions using proportional BMSCs/chondrocytes.[137] A mixture of BMSCs and chondrocytes is employed to regenerate tissue resistance to hypertrophy and ossification for the cartilage zone[137,138] while BMSCs are used in the endochondral region. Next, the chondroinductiveness of the platform and cell design is evaluated under dynamic compression (DC). As a result, the entire substrate surface is covered by new tissues. Col X and a high concentration of calcium are detected from the subchondral region, whereas SZ markers such as Col II and lubricin are observed from the hyaline cartilage part (Figure 5b). Even though the sGAG content reaches that of the native tissue under dynamic condition, the level of expressed collagen is still lower than that of the natural counterpart. Nonetheless, the design can keep the oriented col-

lagen fibers parallel to the surface in the SZ and perpendicular to the surface in deeper zones (Figure 5c,d).[137] Nonetheless, in vivo implantation of this platform based on a relevant animal model is necessary to assure the potential functionality of the regenerated zones in real applications.

Application of DC with a specific regime (sine wave at 10% strain amplitude with 1 Hz frequency for 4 h per day, 5 days per week for 3 weeks) to the cell-loaded agarose hydrogel regulates oxygen level, sGAG, collagen, and PRG4 secretion depth-wise through the construct. Although, combination of DC and confinement does not alter sGAG level, however, compared to the unconfined group, collagen secretion is reversed, with more collagen found on the top area which reduced depth-wise. Specifically, on the top region, Col II and PRG4 secretions are elevated while Col I and Col X are decreased.[139] Furthermore, the zonal cartilage configuration is mimicked by confining agarose hydrogel embedded with infrapatellar fat pad-derived stem cells (FPSCs) and applying compression for 3 weeks at ≈10% strain and 1 Hz, for 2 h per day and 5 days per week.[140] The results indicate that, only hydrogel confinement or compression may not be adequate to boost chondrogenesis, especially for the hydrogel with a height of 4 mm. The combined stimuli do not alter total ECM deposition significantly, but the SZ mimics that of the native AC since the Col II and PRG4 are secreted more, whereas the GAG expression is not significant. The dynamic modulus of the construct increases from 0.96 to 1.45 MPa after exposure to DC. By this approach, the oxygen content decreases to an acceptable level for chondrogenesis,[141] while the glucose level continues to be safe.

3.2.3. Shear Stress

Daily activities impose shear stress on chondrocytes which affects their proliferation, degeneration, ECM production, and up/downregulation of some genes.[142,143] Imposing dynamic culture through medium stirring results in higher expression of chondrogenic biomarkers.[144] Shear stress can be applied to the construct through fluid flow[145] or directly to the whole platform[146] by which the nutrition transport within the construct may increase. However, by fluid flow, the difference between the sensed stress in the outer and inner parts of the construct would be larger compared to the other case, altering the structural integrity and favorable gene expression significantly.[147] Therefore, applying shear stress in a controllable manner should be investigated to ensure reliable and favorable results.[148,149]

The effects of shear stress alone or when combined with other mechanical stimuli like compression and HP on cartilage restoration have been studied.[150,151] Furthermore, the impact of combined mechanical stimuli on minimizing the shear stress catabolic effects have been explored in several works.[152–154] However, limited number has been focusing on the zonal arrangement of hyaline cartilage. For example, in the work done by Tee et al.,[155] a microfluidic device is developed, and shear stress is applied to expand chondrocytes derived from different cartilage zones while retaining their unique size and morphology. Given the complex and graded features of the cartilage zones and variations in the size and morphology of chondrocytes, the use of chondrocytes from the exact targeted zone is desired for cartilage repair. Unfortunately, the availability of primary chondrocytes is limited and probable phenotypic changes in chondrocytes during in vitro expansion hamper the effectiveness. After sorting the on-chip expanded chondrocytes according to their size, it is realized that, upon the dynamic culturing conditions, their morphology remains unchanged, while expressing more hyaline cartilage biomarkers. When the sorted chondrocytes are cultured in 3D fibrinogen hydrogels, the ones related to the specific cartilage zones express zone-related markers.[155] The same approach is applied recently[156] to investigate the performance of zonal-sorted chondrocytes through expansion-sorting strategy when loaded within fibrin hydrogel in vivo. Here, before expansion-sorting, chondrocytes were undergone dynamic culture with dynamic microcarrier and shear stress was applied to the cells followed by static culture. In vivo results indicate the positive impact of this method as the morphology of the cells in DZ, the thickness of the regenerated tissue, the PRG4 distribution, distinct zonal differences, PGs secretion, and their distribution appear more similar to that of the natural cartilage.

Another application of shear stress for cartilage zone-specific TE is demonstrated by Chen et al.[157] wherein SZ is successfully mimicked through applying shear stress via fluid flow on the surface of an agarose gel containing chondrocytes. The motion-induced shear stress is applied by stirring the culture medium in a half-square wave for 40 min (0–25 rpm at 0.004 Hz) followed by a steady stirring at 25 rpm for the remaining time of the day. After applying this regime for 2 weeks, the nominal shear stress of 0.12 Pa is applied to the platform surface. As a result, higher amounts of Col II, PGs, and PRG4 are secreted compared to the static mode without any change in Col I content. Also, the morphology of chondrocytes and collagen Fiber alignments are more resembling the natural SZ; flattened and parallel to the surface, respectively.

Although some detrimental impacts of shear stress on chondrocytes such as matrix degradation and downregulation of chondrogenic genes have been observed,[158–160] Salinas et al.[161] have shown that by applying a specific shear force regimen, chondrocytes proliferate considerably leading to promoted neocartilage formation. Although this study did not deal with each cartilage zone individually, however, the in vivo outcome indicates the effectiveness of the wisely selected shear stress regime when accompanied with bioactive factors including TGF-β1 and LOXL2 for cartilage TE. Even though the results provide valuable clues about ECM-derived cartilaginous structures and adjustment of mechanical properties of the scaffold-free neocartilage according to the defect properties, additional evaluations using animal models applicable to cartilage/osteochondral diseases will be beneficial.

3.3. Biological/Chemical Cues

Exposing cells to an array of biological or chemical signals that exist naturally in the native cartilage ECM recruits and regulates the cellular response for cartilage repair.[162–164] The sustained interaction between cells and adjacent ECM allows biological signals transfer between the extracellular and intracellular environment leading to improved tissue remodeling. CS, HA, and Col II are

examples of biological factors incorporated in cartilaginous scaffolds to promote stem cell chondrogenesis by boosting the tissue specificity.[78] Manipulation of the pathways by delivering soluble signals such as GFs, cytokines, chemokines, and hormones accelerates tissue healing. After diffusion in the cell microenvironment, they are distinguished by the specific cell surface receptors. Thus, cells regulate the signalling pathways and influence their own and other cell functions through autocrine and paracrine signalling, respectively.[165]

3.3.1. Growth Factors

GFs are soluble signaling molecules based on polypeptides/proteins that are secreted by cells. They not only govern cell proliferation, migration, and differentiation, but also control ECM production.[33] Although the recombinant forms of GFs are directly injected into the damaged site or administered systematically in clinical practice, the large molecular size, slow tissue infiltration, short half-life, and possible systemic toxicity limit their application. These issues have been addressed by employing polymeric-based materials as drug carriers in cartilage TE. TGF-β and correlating bone morphogenic proteins (BMPs), IGFs including insulin and FGF are the main classes of GFs that have been exploited in chondrogenic studies.[166]

Immobilization of specific GFs in different zones of the layered scaffold is an attractive strategy to stimulate differentiation of MSCs in each layer.[167] GFs stimulation of cell-laden photoresponsive hydrogels derived from fetal (f-CarMa) and adult (a-CarMa) bovine cartilage ECM shows promising results in differentiation of hMSCs into zone specific chondrocytes. The SZ phenotype chondrocytes are achieved when cells with large densities are encapsulated in f-CarMa and exposed to the chondrogenic medium supplemented with BMP-7 in the presence of TGF-β1. However, when cells with low densities are incorporated in a-CarMa, they differentiate into the CZ chondrocyte phenotype in the culture with chondro-inductive medium/TGF-β1 and sequential stimulation with Indian hedgehog (IHH). Stimulation of hMSCs-laden CarMa (fetal/adult) with insulin-like GF1 (IGF-1) produces the MZ phenotype chondrocytes with intermediate cell densities. Incubation of cell-laden constructs with medium containing BMP-7 and subsequent exposure to IGF-1 produce the MZ phenotype, whereas sequential addition of IHH into the pre-cultured samples in BMP-7 and IGF-1 results in maturation of hMSCS and CZ phenotype formation.[168]

In autologous chondrocyte implantation (ACI), chondrocytes should be passaged serially to achieve enough cell number, resulting in loss of chondrogenic properties. Nevertheless, re-differentiated chondrocytes cultured with TGF-β3 can preserve the chondrogenesis ability which cannot be accomplished by other GFs. According to Bianchi et al.,[169] implantation of fibrin gel encapsulated with pre-treated chondrocytes with TGF-β3 into the rabbit full osteochondral defect regrows the hyaline cartilage compared to using nondifferentiated chondrocytes. In this study, the tissue granulation and vascularization are associated with TGF-β3 treatment. The resulted tissue from this group is stained less strongly for PGs, however, the ICRS II score is significantly higher than the repaired tissue from non-differentiated chondrocytes. Nevertheless, inducing vascularization by specific GFs like VEGF should be avoided when engineering cartilage tissues as they can divert chondrogenic conditions into osteogenic ones.[170,171]

Karimi et al.[64] have shown that the mechanical and biochemical signals synergistically promote the zonal lineage commitment of encapsulated hMSCs in the SPELA gels. The cell density and stiffness of the SZ, MZ, and CZ are simulated and when the soft gel (80 KPa modulus, 60 Mcells mL^{-1}) is exposed to TGF-β1 (3 ng mL^{-1}) and BMP-7 (100 ng mL^{-1}), the SZ markers are upregulated. In contrast, lowering the cell density to 15 Mcells mL^{-1} in the stiffest hydrogel (320 MPa modulus) results in the expression of CZ markers using 30 ng mL^{-1} of TGF-β1. To make the MZ-like tissue, the hydrogel modulus and cell density are adjusted to 2.1 MPa and 20 Mcells mL^{-1}, while the samples are cultured with 30 and 100 ng mL^{-1} of TGF-β1 and IGF-1, respectively.[64] To mimic the fibrillar morphology of the CC ECM, electrospun PLA nanofibers are aligned perpendicular to the surface. Although promising in vitro results have been observed, integrating these layers into one scaffold and assessing the cell fate after in vivo implantation are necessary to improve the outcome.[64]

Recently, Qiao et al.[42] have made a stratified fiber-reinforced hydrogel to simulate the cartilage SZ and DZ with the adjacent subchondral bone (**Figure 6**a–g). The zone-specific GFs are delivered by MSCs-laden GelMA which is integrated with the melt electrowritten triblock polymers of PCL and PEG (named PCEC) that possess zone-dependent topological cues. The PLGA spheres loaded with TGF-β1 and BMP-7 are placed in the superficial layer to attain favorable lubrication by inducing the expression of SZP, whereas only the TGF-β1 carriers are incorporated into the deep layer to maintain chondrogenic differentiation. Osteogenic differentiation is mediated via the BMP-2 pathway for the subchondral bone part using BMP-2-loaded microspheres. The bone-mimicking layer shows a compressive modulus of 55.8 ± 5.4 MPa close to that of native spongy bone, whereas the modulus of the bi-layered cartilage-like tissue (964.2 ± 56.8 kPa) reaches the level of native cartilage. SZP expression is the highest in the superficial layer and the highest aggrecan and OCN deposition are observed from the deep and subchondral bone layers, respectively. Despite irregular growth of MSCs and randomly organized cytoskeletons in the deep and bone regions, the cells and cytoskeletons are more uniformly aligned along the long axis of the fibers in SZ. 6 months after implantation of the tri-layered scaffold into rabbit osteochondral defect models, a hyaline-mimicking cartilage possessing a wear-resistant surface integrated with the subchondral bone is observed.[42]

Apart from developing different layers of AC, CC as a transition layer between AC and subchondral region plays crucial roles. In this regard, growth and differentiation factor-5 (GDF-5) which belongs to the BMP family can be used for in vivo cartilage maturation and mineralization enhancement. This GF increases ALP activity and subsequently mineralization and hypertrophic activity. Supplementation of 150 ng mL^{-1} GDF-5 into the chondrogenic medium enhances the porcine BMSCs hypertrophic activity in vitro.[172] In the ectopic bone formation experiment by subcutaneous placement of fibrin constructs containing pre-treated BMSCs with GDF-5 on the dorsal area of a nude mice, considerable cartilage formation is seen from both the GDF-5-treated and control groups. All the hypertrophic biomarkers are at the same levels except for ALP which is significantly higher in the

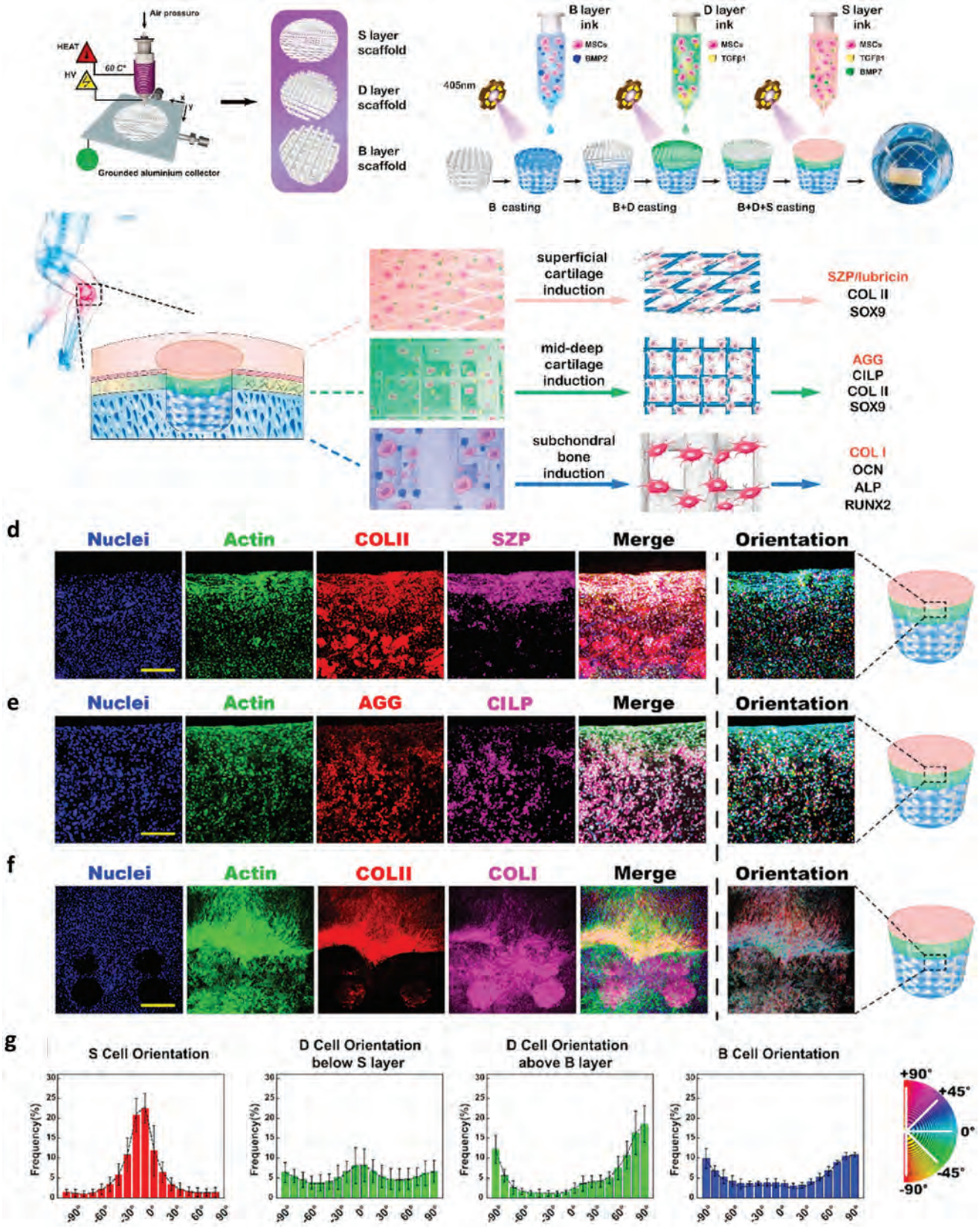

Figure 6. Schematic illustration of the preparation of the multi-layered composite. a) Fibrous networks produced by meltelectrowriting for the superficial (S), deep (D), and bone (B) layers. b) Integration of the three layers. The cells and GF-loaded GelMA precursor solution of the corresponding zone diffuse

GDF-5-treated group. The results are verified by μ-CT evaluation showing 1.6-fold larger bone volume than the control. Therefore, to further analyze the capability of GDF-5 to form CC, a three-layered construct made from a bone disc, a starPEG-heparin hydrogel mixed with fibrin gel containing GDF-5-treated BMSCs, and a cell-free fibrin hydrogel is placed subcutaneously in the dorsal area of a nude mice. After 7 weeks in vivo, a CC layer is formed flawlessly in GDF-5-treated group without cartilage detachment unlike the one formed in the control group. The layer consists of Col X with strong mineralization activity. These results are promising in the efforts to further examine the developed layered scaffold in cartilage related animal models in order to more effectively identify potential applications in cartilage TE.

3.3.2. Hormones

Hormones are effective modulators of the cell microenvironment that can activate or inhibit various molecular pathways (anabolic/catabolic activities) by which chondrogenesis can be governed.[173] Triiodothyronine (T3), a hormone that selectively promotes chondrocytes mineralization, is beneficial when designing CC.[174] DZ chondrocytes are treated with T3 (25 nM) for 3 days to induce hypertrophy by stimulating the ALP activity and upregulating the Col X expression. The stimulated cells are then encapsulated in agarose hydrogels reinforced with nano/micro-sized HAp particles and cultured for 2 weeks to generate CC. The higher shear modulus of micro-HAp hydrogels is related to the higher matrix content. This can better emulate the interplay between collagen and PGs responsible for strengthening the cartilage shear. Hence, both HAp and T3 synergistically induce the chondrocytes hypertrophy.[175]

The parathyroid hormone-related protein (PTHrP) can be utilized to design the microenvironment resembling physiological signaling cues in vivo to modulate the fate of stem cells. PTHrP is a regulator of chondrocytes hypertrophy and undergoes maturation through endochondral development.[176] It preserves chondrocyte proliferation while delaying hypertrophy via binding to PTHrP receptors. Spatial PTHrP signaling is applied to fibrin-poly(ester-urethane) scaffolds by seeding adenovirally transduced MSCs (AdPTHrP) on the composite wherein un-transduced MSCs are incorporated evenly. AdPTHrP overexpresses PTHrP to boost GAG deposition, chondrogenesis, and secretion of TGF-β1 by MSCs and provide differential effects on chondrogenesis and hypertrophic gene expression.[176]

3.3.3. Small Molecules

Considering the higher stability and lower cost of small molecules compared to GFs, their application in cartilage repair has aroused interest.[177] KGN, a small biomolecule that selectively stimulates chondrogenesis of MSCs, is a good example. Highly aligned core-shell nanofibers are electrospun coaxially to emulate the morphology of cartilage SZ. PCL is used as the shell materials and poly(glycerol sebacate) (PGS) loaded with KGN serve as the core component. Sustained delivery of KGN for 21 days (0.32 ± 0.03 μg KGN mg^{-1} of scaffold) spurs proliferation and chondrogenesis of human BMSCs (hBMSCs). Enhanced expressions of sGAG, SOX-9, Col II, ACAN, and more importantly, substantial upregulation of PRG4 even in the absence of TGF-β3, confirm lubrication on the articulating surface.[177]

A combination of biological stimuli including delivering TGF-β1 and KGN by PLGA microspheres and polylysin-heparin sodium and structural design (oriented porous structure) has been reported to develop cartilage-like SZ and transitional layers.[178] Collagen, chitosan, and HA sodium (HAS) are employed as building blocks of the SZ to mimic cartilage ECM with potential downregulation of inflammatory factors using HAS and incorporation of KGN carriers. Meanwhile, collagen, chitosan, and silk fibroin combined with TGF-β1-loaded particles are used for the second zone. Release of both biological cues synergistically increases cell proliferation in vitro. After in vivo implantation of the dual-layer scaffold into the rabbit knee osteoarthritic cartilage defect model, good integration with the host tissues is observed as manifested by a cell morphology analogous to that of native tissues. The endogenous BMSCs migrate from the broken subchondral bone to the middle layer due to the positive TGF-β1 effects on cell adhesion and proliferation followed by chondrogenesis and infiltration into the SZ by KGN signaling. Despite promising results in vivo, enhancement of the scaffold compressive modulus (1.2 KPa) is preferred.[178]

Incorporation of KGN in a thermogel based on PLGA-PEG-PLGA, provides full thickness cartilage tissue regeneration with elevated mechanical properties in vivo. The expressed GAGs and Col II in regenerated tissue is more than 90% of the normal tissue.[179]

In another attempt,[22] KGN is encapsulated in a thermosensitive chitosan hydrogel modified with *N*-(β-maleimidopropyloxy) succinimide ester (BMPS) with a shear modulus of 78 kPa. Continuous KGN release from this injectable hydrogel for a month and upregulation of SOX-9, Col II, aggrecan, and GAG expressed by hAMSCs along with fast gelation show a good potential to be used in SZ/MZ defects. Furthermore, considering the changes in the AC shear modulus depth-wise from 50 to 250 kPa, a series of hydrogel formulations are developed, and statistical models are generated as functions of gel ingredients to predict the properties such as the shear modulus. This renders it possible to tailor the mechanical properties of scaffolds based on the defect location in order to provide the suitable shear modulus within the range of 1.4 to 76 kPa.[22] Additionally, KGN is encapsulated in starch microspheres produced by a droplet microfluidic chip for better gradual drug release and chondrogenesis effect. The KGN-loaded particles are subsequently incorporated in a BMPS-modified chitosan thermogel containing diclofenac sodium

into the fibrillar layers and UV crosslinked to make the tri-layered structure. c) Schematic figure showing the application of the composite in zone-specific osteochondral tissue regeneration. d–f) Expression of zone-dominant biomarkers (SZP for the S layer and CILP for the D layer) and Col II and aggrecan (Agg) in the chondrogenic layers (S and D) ((d) and (e), scale bar: 200 μm) and the expression of Col II for the cartilage zones and Col I for the osteogenic region at the osteochondral junction for f) Tri-layer constructs upon 28 days induction (scale bar: 400 μm). g) Orientation of the cells in the S, superficial D, deep D, and B zones presented in the frequency distribution histogram. Reproduced with permission.[42] Copyright 2021, Elsevier.

(DS)-loaded halloysite nanotubes. Considering the ability to co-deliver KGN for chondrogenesis and DS for pain reduction in addition to the high shear modulus of 167 kPa, this system can regenerate defects in cartilage MZ.[180]

As discussed here, recently published papers only used KGN for cartilage repair, however, other small molecules could be considered for this purpose. For example, BNTA is a small molecule which has ECM modulatory properties.[181] It can highly affect the chondrocytes derived from osteoarthritis patients by stimulating the ECM expression while curbing inflammatory mediators. Besides this, small molecule 6 with sulfunomide has been employed as an agent that boosts chondrogenesis of hASCs. Conjugation of this molecule to biopolymers could be utilized in regeneration of AC zones and investigated in vivo.[182] RCGD 423 (regulator of cartilage growth and differentiation) is another potential small molecule for rapid cartilage healing that is also able to suppress inflammation.[183] Other small molecules and compounds that show potential for cartilage repair have been reviewed by Li et al.[184] which could pave the road for designing novel cartilaginous scaffolds.

3.3.4. ECM

ECM proteins governing the cellular behavior, can be used alone or in combination with other biomaterials to develop biologically and functionally relevant tissue alternatives that mimic the native cartilage. HA is one of the main components of cartilage ECM which has been utilized in various formats for zonal cartilage TE. A 3D-printed structure is made from HA and decellularized ECM (dECM) according to the shape of cartilage lesion accompanied with thiolated-HA on the top to resemble SZ.[185] dECM has an undeniable impact on the final structure of the regenerated tissue.[186] For example, the collagen alignment of decellularized mature porcine AC, guides the collagen fibers secreted by the human infrapatellar fat pad derived stem cells (hiFPSCs) after recellularization of the scaffold which are arranged perpendicular to the surface.[187]

A three-layer PEG gel has been fabricated wherein CS and matrix metalloproteinase-sensitive peptides (MMP-pep) are used in the first layer to develop an SZ-like tissue. Incorporation of CS into the second layer and HA into the bottom layer gives rise to TZ and DZ-resembling tissues, respectively. Gradual decrease of Col II with moderate upsurges in Col X, PGs content, and compressive modulus from the top to bottom layer validate the roles of the materials composition in spatial tailoring of the scaffold biochemical and mechanical properties.[188,189] In another attempt, hyaluronic acid methacrylate (HA-MA) and GelMA are incorporated with different chondrocyte densities for cartilage repair purpose showing that, GelMA with higher cell density (25 Mcells mL^{-1}), provides higher expression of Col I, as a sign of premature chondrocyte phenotype.[190]

Furthermore, different formulations of photocurable, interpenetrating hydrogels made of HA, CS, and PEG have been investigated under normaxia and hypoxia conditions to optimize zone-dependent chondrogenesis of hBMSCs. Based on the observed differences from single layers, a spatially-patterned trilayered construct in terms of sGAG and collagen distribution is developed under normaxia for better ECM production. Combining 19% PEG diacrylate (PEGDA) with 1% HA-MA results in the most promising Col II with low sGAG, making it suitable for the SZ. The formulation of 9% PEGDA with 10% CS-MA and 1% HA-MA exhibits high Col-II with higher sGAG concentration which is appropriate for the TZ. The middle-like layer is composed of 10% PEGDA + 10% CSMA in which Col X and sGAG are the highest.[191]

HA-based hybrid scaffolds are made with the goal of inducing zonal-specific cellular morphology and ECM composition. Two layers of HA hydrogels enveloping specifically or randomly orientated PLA nanofibers are designed for SZ and MZ, whereas the gel with multiple vertical channels is developed for the DZ. After cell culturing on the SZ for 14 days, more proliferation of chondrocytes with an elongated shape and lower Col II and GAG and higher Col I compared to MZ are observed. In the MZ, the cells express more Col II while clustered, but in the DZ, the highest GAG deposition with lowest Col I expression and cell proliferation are observed. When the layers are assembled, the cells are aligned in the SZ, randomly aggregate in the MZ, and are oriented in columns in the DZ.[192]

A multi-layer osteochondral scaffold wherein the cartilage ECM composition is mimicked using Col I and HA as building blocks of the chondral compartment has been fabricated. The osseous part is composed of Col I and HAp which promotes osteogenesis by secreting phosphate ions (PO_4^{3-}) for intracellular uptake. The structure provides the same architectural features in osteochondral tissues. Despite the gradual change in the morphology, composition, and mechanical properties from the superficial to bone-imitating layers, the scaffold properties should be investigated further in vitro and in vivo.[193]

Benefiting from combination of ECM proteins and GFs preserved in dECM as building blocks of our scaffolds is an efficient way to tackle the limited cartilage regeneration capacity.[37] A nanofibrous scaffold derived from cartilage dECM is made to mimic the cartilage biochemical composition while emulating the DZ collagen alignment.[194] Vertically aligned and interconnected microtubules are fabricated by the TIPS technique. Although the fibrillar morphology and cell orientation along the microtubules mimic the DZ, the cultured MSCs exhibit a mostly ellipsoidal/spindle shape unlike the spherical chondrocytes in the DZ.[194] Even though some preliminary in vivo studies have been performed by implantation of the scaffolds subcutaneously into the dorsal of nude mice, further evaluations using the relevant animal models are needed.

Whether or not exposure of cells to ECM zone-specific molecules preferentially direct human articular chondrocytes (hACs) toward the zone-dependent phenotypes is important to the design of functional native-like cartilage substitutes. The effects of cartilage zone-specific ECM signaling molecules on regulation/maintenance of the hAC phenotypes have been studied in monolayers, pellets, and 3D cell cutlers by Grogan et al.[195] The molecules include biglycan, decorin, and tenascin C for the SZ. Col II and HA are explored for the middle and DZ-specific ECM molecules, whereas osteopontin is used for the DZ. ALG hydrogels combined with each biomolecule are used in the 3D cell cultures (8 Mcells mL^{-1}) where the concentration of ECM proteins is adjusted to 1 μg mL^{-1} except HA which is 1 mg mL^{-1}. Hydrogels supplementation with HA is most effective in inducing neocartilage generation considering the enhanced aggrecan and COL2A1

in addition to decreased COL1A1 compared to the controls. Col II supplementation presents an increasing trend in the COL2A1 expression despite the large variability. Additionally, both decorin and biglycan suppress PRG4 expression compared to the controls. Results reveal that, application of only one/purified ECM molecule is not ideal in promoting the zone-specific chondrocyte phenotypes. Instead, utilizing the whole or zonal cartilage ECM is more promising in modulating the zone-dependent gene expression profiles.[195]

A two-zone construct made of GelMA, gellan gum, and methacrylated HA is 3D-printed to simulate the SZ and MZ/DZ of AC.[196] The AC progenitor cells (ACPCs) harvested from the cartilage SZ are used in SZ and MSCs are incorporated into the second layer to develop the MZ/DZ-resembling gel. Improvement of the limited zonal difference between the layers and hydrogel mechanical properties leads to better tissue functions.[196]

GelMA, HA-MA, CS-aminoethyl methacrylate (CS-AEMA), and ALG have been used as photocurable bioinks in a microfluidic extruder capable of hydrogel mixing and 3D printing of gradient hMSCs- and hACs-laden matrices for osteochondral defects.[197,198] Two different bioinks are produced for hyaline and CC. The hyaline cartilage-mimicking layer is composed of 4% w/v ALG, 6% w/v GelMA, and 4% w/v CS-AEMA with a 3:1 ratio of hMSCS:hACs and yields the hyaline phenotype with differentiated hMSCs. To induce biomimicry in the CC, the hyaline cartilage formulation is mixed with 0.5% w/v HA-MA and 0.5% w/v β-tricalciumphosphate (β-TCP) microparticles. The layer is encapsulated only with hMSCs and significant upregulation of ALPL and COL10A is accomplished.[197] Besides this, ALG-GelMA with 0.5% w/v β-TCP is utilized for CC through 3D-printing procedure. Although β-TCP acted as a physical crosslinker, however higher amount of it can further reduce the mechanical properties of final product.[199]

Recently, ECMs derived from xenogeneic AC and growth plates have been used as building blocks of a two-phasic construct to provide a functional osteochondral unit with temporal properties resembling AC and underlying bone, respectively. Accordingly, arrays of regulatory proteins matching the bone and cartilage in each corresponding layer direct differentiation of stem cells in vitro.[200] 12 months after implantation of the graded scaffolds into critical-size caprine osteochondral defects, the architecture of the newly formed collagen network is analogous to that of natural condyles and the regenerative properties are better than commercial scaffolds as controls. Despite promising tissue remodeling upon implantation without negative immune response, further investigations are needed to validate their clinical potential.

In another work done by Kunisch et al.,[201] a stable calcified layer is fabricated and the growth toward the AC layer is prevented. A zonal construct made from pellet-like pre-cultured porcine BMSCs on the bottom and starPEG/heparin hydrogel with chondrocytes on top is used in the ectopic in vivo experiments using the dorsal site of nude mice. Heparin, a natural GAG, prevents the calcification of the hydrogel and growth of the CC layer toward the AC zone. For comparison, by using fibrin hydrogel instead of starPEG/heparin, less mineralized cartilage is formed with smaller contents of Col II and the presence of ALP and Col X is determined in half of the gel. Application of the starPEG/heparin hydrogel on top of the BMSCs pellet prevents ossification of MSCs. While in the non-zonal construct, the pellet finally progresses to the mature bone after 12 weeks and is depleted from Col II. However, in vivo studies based on a relevant animal model for cartilage repair can reveal the functions of this system more realistically.

To achieve anisotropic zonal distributions of ECM, Ren et al.[162] have used chondrocytes gradient densities in a 3D printed Col II hydrogels to replicate the cell gradient densities in cartilages. The ratio of the chondrocyte densities in the SZ, MZ, and DZ is adjusted to 3:2:1 to match that of the human femoral condyle. This results in reduction of GAG, Col II, and PRG4 from the top to bottom layers, although in natural cartilage, the sGAG content increases from the SZ to deeper layers.[162]

Although zonal cartilage TE with the application of biopolymers with different physical properties are still in the early stages and even with some contradictory results concerning the benefits of these approaches, in the recent decade, few matrix-associated ACI for cartilage tissue treatment have been reached to clinical trials and even available in the markets. These scaffolds are made from different biopolymers such as collagen I,[202] HA,[203] and chitosan-based hydrogels,[14] and usually accompanied with autologous chondrocytes, in vitro expanded or not.[204,205] In the most cases the outcome has been better compared to the available techniques such as microfracture, nonetheless, there is no preference between them and apprehensive study within large cases are needed.[206,207] For example, a recent study on one of the approved matrices, CaReS, shows that 12 weeks in vitro cell growth on this platform in a standardized bovine punch model, enhances the PGs deposition and overall cartilage tissue regeneration.[208] These platforms can be effective mostly in grade III of cartilage lesion, while CaReS is stated to be effective on grade IV. However, in severe OA cases, where most of the cartilage is already damaged or worn out, they are still not practical solutions.

4. Conclusion and Prospective

The AC avascular nature, depth-dependent physio-mechanical properties, composition, and cell phenotypes present challenges to the regenerating process. In many cases, the regenerated tissues are unstructured and the properties are quite different from those of the natural cartilage.[209] The lack of biological and physical signals or mechanical cues imitating the joint dynamic microenvironment for cell guidance are the main reasons underlying disappointing results in long-term follow-up. Although changing the culturing conditions by supplementing biomolecules/GFs or applying various mechanical loadings have produced some success in cartilage repair in animal studies, the optimal conditions have not been identified for zonal organization of cartilages.

This review summarizes the recent development of polymeric scaffolds with emphasis in mimicking the different AC zones using physical, mechanical, and biological/chemical cues. Zonal organization of the neo-tissues in terms of the final cellular fate, morphology, orientation, ECM composition, and physio–mechanical properties in these constructs are described. Despite recent advances in this field, the materials and techniques are still not close to clinical acceptance because most of the developed scaffolds do not fully mimic the natural cartilage configuration and very few of them have been tested in vivo using rele-

vant animal models for cartilage repair. Indeed, the translation of the bench works into real clinical practice is not accomplishable without substantial evidence on long-term efficacy and safety in appropriate large animal models.

One solution is to design culturing conditions suitable for expansion of chondrocytes while preserving their phenotypes. Microfluidics and advanced cell sorting systems make it more feasible to employ zone-dependent chondrocytes in the scaffolds with relevant tissue-scaled cell densities. This facilitates spatial patterning of the constructs not only with zone-specific chondrocytes, but also with the corresponding ECM composition with the relevant chondrocytes subpopulations. Furthermore, delivering the right zonal GFs in an orchestrated manner with the applicable concentration must be considered which necessitates smart drug delivery systems. Alternatively, we can take advantage of the zonal cartilage dECM to deliver a pool of ECM signaling molecules and GFs related to the targeted region. The hypoxic environment of cartilages along with the mechanical loads that are routinely applied to tissue should be investigated systematically because they are key regulators of cell functions which can be provided by bioreactors.

Although some researchers have mimicked the AC zones separately, assembling the layers is important to altering the scaffold composition and physio–mechanical properties between layers and offering a tissue-scalable construct. In the meantime, vascularization needs to be confined beneath the cartilage tidemark and triggered in the subchondral bone region. Proper integration of scaffolds with adjacent host tissues is crucial to mechanotransduction thus demanding that the scaffolds have the proper biological properties. Most of the previous studies have used animal-derived cells but it is important to obtain the same results using cells from patients because the ultimate objective is clinical adoption.

So far, very few products have been approved and commercialized for cartilage repair.[10,14,202,203,205,210,211] Although, all of them show significant cartilage regeneration compared to conventional methods like microfracture, however, they are mainly suitable for grade III cartilage lesions and in the worst scenarios like advanced osteoarthritis, they are still impractical. Besides the unsatisfactory clinical outcome, other obstacles include the cost of reagents and production process, difficulty in scaling up production while maintaining the quality, sterility, consistent manufacturing, shelf life, storage, and shipping conditions. The NeoCart implant (Histogenics, Waltham, Massachusetts), BST-CarGel (Piramal Healthcare Inc., Laval, Quebec, Canada), Chondro-gide (Genzyme Biosurgery, Kastrup, Denmark), and Hyalograft C (Anika Therapeutics Inc., Bedford, MA, U.S.A.) are some examples of commercial polymeric scaffolds used in cartilage restoration.[212–214]

All in all, in order to achieve better tissue functions and smooth the load transfer through scaffold defects, we need to specifically design scaffolds optimized for the targeted zone with unique features analogous to those of the native cartilage layers. Most of the products on the market are designed for cartilage defects without considering the zonal location and so they do not fully emulate all the cartilage regions.[214] On the heels of recent advances in biofabrication technologies like 3D printing, microfluidic platforms for cell culture and sorting, and smart drug delivery systems, it is expected that in the near future, scientists will be able to develop personalized cartilaginous tissues with the native AC configuration by taking all the exogenous stimuli into account. Meanwhile, the potential interactions of these stimuli with each other and final properties of the neo-tissue must be considered to control the conditions in a more accurate way.

Acknowledgements

D.D.-B. and B.M. contributed equally to this work. The authors acknowledge funding supports from the HK ITC (ITC-CNERC14SC01), the Hong Kong RGC (GRF 16308818, GRF 16309920, and GRF 16309421), the Partnership Research Programme and the Research Talent Hub, Innovation and Technology Fund, Hong Kong SAR (Ref No: PRP/090/20X), the Research Matching Grant Scheme (RMGS), the Area of excellence (Ref. No. AoE/M-402/20) University grants committee, the Centre for Neuromusculoskeletal restorative medicine (Ref. No. CT1.1) Health@InnoHK program, the Innovation technology commission, the Hong Kong SAR, the University Grants Committee, the HKSAR, the Shenzhen – Hong Kong Innovative Collaborative Research and Development Program (SGLH20181109110802117 and CityU 9240014), as well as the City University of Hong Kong Donation Research Grant (DON-RMG 9229021).

Conflict of Interest

The authors declare no conflict of interest.

Keywords

articular cartilage zones, biological and chemical cues, cartilage tissue engineering, mechanical cues, physical cues

Received: October 8, 2022
Revised: December 19, 2022
Published online: January 18, 2023

[1] A. J. Sophia Fox, A. Bedi, S. A. Rodeo, *Sports Health* **2009**, *1*, 461.
[2] B. R. Rawal, R. Ribeiro, M. Chouksey, K. Tripathi, *J. Med. Sci* **2013**, *13*, 615.
[3] C. Vinatier, D. Mrugala, C. Jorgensen, J. Guicheux, D. Noël, *Trends Biotechnol.* **2009**, *27*, 307.
[4] A. R. Armiento, M. J. Stoddart, M. Alini, D. Eglin, *Acta Biomater.* **2018**, *65*, 1.
[5] Z. Ge, C. Li, B. C. Heng, G. Cao, Z. Yang, *J. Biomed. Mater. Res., Part A* **2012**, *100 A*, 2526.
[6] K. E. Kuettner, *Clin. Biochem.* **1992**, *25*, 155.
[7] American Academy of Orthopaedic Surgeons Management of Osteoarthritis of the Knee (NonArthroplasty) Evidence-Based Clinical Practice Guideline. https://www.aaos.org/oak3cpg
[8] A. R. Armiento, M. Alini, M. J. Stoddart, *Adv. Drug Delivery Rev.* **2019**, *146*, 289.
[9] D. C. Crawford, C. M. Heveran, W. D. Cannon, L. F. Foo, H. G. Potter, *Am. J. Sports Med.* **2009**, *37*, 1334.
[10] D. C. Crawford, T. M. DeBerardino, R. J. Williams, *J. Bone Jt. Surg.* **2012**, *94*, 979.
[11] T. M. Deberardino, *Sports Med. Arthrosc. Rev.* **2015**, *23*, e23.
[12] A. C. Mascarenhas, A. Kusanagi, E. B. Blahut, J. Johnson, L. J. Berlowitz-Tarrant, S. Mizuno, presented at 46th Annual Meeting, Orthopaedic Research Society, Orlando, FL, March **2000**.

[13] S. Méthot, A. Changoor, N. Tran-Khanh, C. D. Hoemann, W. D. Stanish, A. Restrepo, M. S. Shive, M. D. Buschmann, *Cartilage* **2016**, *7*, 16.
[14] M. S. Shive, W. D. Stanish, R. McCormack, F. Forriol, N. Mohtadi, S. Pelet, J. Desnoyers, S. Méthot, K. Vehik, A. Restrepo, *Cartilage* **2015**, *6*, 62.
[15] W. D. Stanish, A. Restrepo, P. B. Macdonald, N. Mohtadi, P. H. Marks, M. Malo, J. Desnoyers, R. G. Mccormack, S. Pelet, F. Forriol, M. D. Buschmann, M. S. Shive, *Arthroscopy* **2011**, *27*, e168.
[16] R. Yang, F. Chen, J. Guo, D. Zhou, S. Luan, *Bioacta Mater.* **2020**, *5*, 990.
[17] N. Mahmoudifar, P. M. Doran, *Trends Biotechnol.* **2012**, *30*, 166.
[18] F. T. Moutos, F. Guilak, *Biorheology* **2008**, *45*, 501.
[19] H. Kwon, W. E. Brown, C. A. Lee, D. Wang, N. Paschos, J. C. Hu, K. A. Athanasiou, *Nat. Rev. Rheumatol.* **2019**, *15*, 550.
[20] T. Stampoultzis, P. Karami, D. P. Pioletti, *Curr. Res. Transl. Med.* **2021**, *69*, 103299.
[21] Z. Wang, H. Le, Y. Wang, H. Liu, Z. Li, X. Yang, C. Wang, J. Ding, X. Chen, *Bioacta Mater.* **2022**, *11*, 317.
[22] D. Dehghan-Baniani, Y. Chen, D. Wang, R. Bagheri, A. Solouk, H. Wu, *Colloids Surf. B: Biointerfaces* **2020**, *192*, 111059.
[23] D. Dehghan-Baniani, B. Mehrjou, P. K. Chu, H. Wu, *Adv. Healthcare Mater.* **2021**, *10*, 2001018.
[24] D. D. Baniani, R. Bagheri, A. Solouk, *Carbohydr. Polym.* **2017**, *174*, 633.
[25] F. T. Moutos, L. E. Freed, F. Guilak, *Nat. Mater.* **2007**, *6*, 162.
[26] A. Zelinka, A. J. Roelofs, R. A. Kandel, C. de Bari, *Osteoarthritis Cartilage* **2022**, *30*, 1547.
[27] H. Le, W. Xu, X. Zhuang, F. Chang, Y. Wang, J. Ding, *J. Tissue Eng.* **2020**, *11*, 204173142094383.
[28] K. D. Ngadimin, A. Stokes, P. Gentile, A. M. Ferreira, *Biomater. Sci.* **2021**, *9*, 4246.
[29] L. Zhou, P. Guo, M. D'este, W. Tong, J. Xu, H. Yao, M. J. Stoddart, G. J. V. M. Van Osch, K. K.-W. Ho, Z. Li, L. Qin, *Engineering* **2022**, *13*, 71.
[30] F. A. Müller, L. Müller, I. Hofmann, P. Greil, M. M. Wenzel, R. Staudenmaier, *Biomaterials* **2006**, *27*, 3955.
[31] M. E. Grigore, *J. Tissue Sci. Eng.* **2017**, *08*, 6.
[32] M. Zhu, W. Zhong, W. Cao, Q. Zhang, G. Wu, *Bioacta Mater.* **2021**, *9*, 221.
[33] M. Dang, L. Saunders, X. Niu, Y. Fan, P. X. Ma, *Bone Res.* **2018**, *6*, 25.
[34] G. N. Hall, W. L. Tam, K. S. Andrikopoulos, L. Casas-Fraile, G. A. Voyiatzis, L. Geris, F. P. Luyten, I. Papantoniou, *Biomaterials* **2021**, *273*, 120820.
[35] A. R. Tan, C. T. Hung, *Stem Cells Transl. Med.* **2017**, *6*, 1295.
[36] Y. Liu, G. Zhou, Y. Cao, *Engineering* **2017**, *3*, 28.
[37] Y. Z. García-Carvajal, D. Garciadiego-Czares, C. Parra-Cid, R. Aguilar-Gaytn, C. Velasquillo, C. Ibarra, J. S. Castro Carmo, in *Regenerative Medicine and Tissue Engineering*, (Ed: J. A. Andrades), IntechOpen, London **2013**, Ch. 15.
[38] S. Sharma, A. Panitch, C. P. Neu, *Acta Biomater.* **2013**, *9*, 4618.
[39] M. Keeney, J. H. Lai, F. Yang, *Curr. Opin. Biotechnol.* **2011**, *22*, 734.
[40] J. Oinas, A. P. Ronkainen, L. Rieppo, M. A. J. Finnilä, J. T. Iivarinen, P. R. van Weeren, H. J. Helminen, P. A. J. Brama, R. K. Korhonen, S. Saarakkala, *Sci. Rep.* **2018**, *8*, 11357.
[41] H. Tavakoli Nia, L. Han, I. Soltani Bozchalooi, P. Roughley, K. Youcef-Toumi, A. J. Grodzinsky, C. Ortiz, *ACS Nano* **2015**, *9*, 2614.
[42] Z. Qiao, M. Lian, Y. Han, B. Sun, X. Zhang, W. Jiang, H. Li, Y. Hao, K. Dai, *Biomaterials* **2021**, *266*, 120385.
[43] T. M. Quinn, H. J. Häuselmann, N. Shintani, E. B. Hunziker, *Osteoarthritis Cartilage* **2013**, *21*, 1904.
[44] B. He, J. P. Wu, T. B. Kirk, J. A. Carrino, C. Xiang, J. Xu, *Arthritis Res. Ther.* **2014**, *16*, 205.
[45] K. Miyatake, K. Iwasa, S. M. McNary, G. Peng, A. H. Reddi, *Cartilage* **2016**, *7*, 388.
[46] S. P. Grogan, S. F. Duffy, C. Pauli, J. A. Koziol, A. I. Su, D. D. D'Lima, M. K. Lotz, *Arthritis Rheum.* **2013**, *65*, 418.
[47] H. Akkiraju, A. Nohe, *J. Dev. Biol.* **2015**, *3*, 177.
[48] A. Asari, S. Miyauchi, S. Kuriyama, A. Machida, K. Kohno, Y. Uchiyama, *J. Histochem. Cytochem.* **1994**, *42*, 513.
[49] M.-C. Killen, C. P. Charalambous, *Advances in Medical and Surgical Engineering*, (Eds: W. Ahmed, D. A. Phoenix, M. J. Jackson, C. P. Charalambous), Elsevier, New York **2020**, pp. 71–83.
[50] Y. Zhang, F. Wang, H. Tan, G. Chen, L. Guo, L. Yang, *Int. J. Med. Sci.* **2012**, *9*, 353.
[51] Y. Huang, H. Fan, X. Gong, L. Yang, F. Wang, *Am. J. Sports Med.* **2021**, *49*, 1883.
[52] C. Chen, J. Xie, L. Deng, L. Yang, *ACS Appl. Mater. Interfaces* **2014**, *6*, 16106.
[53] Q. Zhang, Y. Yu, H. Zhao, *Acta Biochim. Biophys. Sin.* **2016**, *48*, 958.
[54] J. Lee, O. Jeon, M. Kong, A. A. Abdeen, J.-Y. Shin, H. N. Lee, Y. B. Lee, W. Sun, P. Bandaru, D. S. Alt, K. Lee, H.-J. Kim, S. J. Lee, S. Chaterji, S. R. Shin, E. Alsberg, A. Khademhosseini, *Sci. Adv.* **2020**, *6*, eaaz5913.
[55] E. Schuh, J. Kramer, J. Rohwedel, H. Notbohm, R. Müller, T. Gutsmann, N. Rotter, *Tissue Eng. Part A* **2010**, *16*, 1281.
[56] J. L. Allen, M. E. Cooke, T. Alliston, *Mol. Biol. Cell* **2012**, *23*, 3731.
[57] C. H. Chen, C. Y. Kuo, Y. J. Wang, J. P. Chen, *Int. J. Mol. Sci.* **2016**, *17*, 1957.
[58] S. Moeinzadeh, S. R. Pajoum Shariati, E. Jabbari, *Biomaterials* **2016**, *92*, 57.
[59] J. He, Y. Du, J. L. Villa-Uribe, C. Hwang, D. Li, A. Khademhosseini, *Adv. Funct. Mater.* **2010**, *20*, 131.
[60] D. J. Huey, J. C. Hu, K. A. Athanasiou, *Science* **2012**, *6933*, 917.
[61] M. A. Kinney, T. C. McDevitt, *Trends Biotechnol.* **2013**, *31*, 78.
[62] X. Tong, J. Jiang, D. Zhu, F. Yang, *ACS Biomater. Sci. Eng.* **2016**, *2*, 845.
[63] D. Guarnieri, A. de Capua, M. Ventre, A. Borzacchiello, C. Pedone, D. Marasco, M. Ruvo, P. A. Netti, *Acta Biomater.* **2010**, *6*, 2532.
[64] T. Karimi, D. Barati, O. Karaman, S. Moeinzadeh, E. Jabbari, *Integrative Biol.* **2015**, *7*, 112.
[65] D. Zhu, X. Tong, P. Trinh, F. Yang, *Tissue Eng Part A* **2018**, *24*, 1.
[66] J. B. Guo, T. Liang, Y. J. Che, H. L. Yang, Z. P. Luo, *BMC Musculoskelet. Disord.* **2020**, *21*, 425.
[67] D. Mitrovic, M. Quintero, A. Stankovic, A. Ryckewaert, *Lab. Invest.* **1983**, *49*, 309.
[68] J. Antons, M. G. M. Marascio, J. Nohava, R. Martin, L. A. Applegate, P. E. Bourban, D. P. Pioletti, *J. Mater. Sci. Mater. Med.* **2018**, *29*, 57.
[69] E. Liu, D. Zhu, E. G. DIaz, X. Tong, F. Yang, *Tissue Eng. Part A* **2021**, *27*, 929.
[70] D. Zhu, P. Trinh, E. Liu, F. Yang, *ACS Biomater. Sci. Eng.* **2018**, *4*, 3561.
[71] C. Li, K. Wang, T. Li, X. Zhou, Z. Ma, C. Deng, C. He, B. Wang, J. Wang, *ACS Appl. Bio Mater.* **2020**, *3*, 4820.
[72] Y. Wu, P. Kennedy, N. Bonazza, Y. Yu, A. Dhawan, I. Ozbolat, *Cartilage* **2021**, *12*, 76.
[73] D. G. O'Shea, C. M. Curtin, F. J. O'Brien, *Biomater. Sci.* **2022**, *10*, 2462.
[74] T. J. Levingstone, A. Matsiko, G. R. Dickson, F. J. O'Brien, J. P. Gleeson, *Acta Biomater.* **2014**, *10*, 1996.
[75] F. G. Lyons, J. P. Gleeson, S. Partap, K. Coghlan, F. J. O'Brien, *Clin. Orthop. Relat. Res.* **2014**, *472*, 1318.
[76] J. P. Gleeson, T. J. Levingstone, F. J. O'brien, US 9072815 B2 **2015**.
[77] T. J. Levingstone, E. Thompson, A. Matsiko, A. Schepens, J. P. Gleeson, F. J. O'brien, *Acta Biomater.* **2016**, *32*, 149.

[78] J. M. Coburn, M. Gibson, S. Monagle, Z. Patterson, J. H. Elisseeff, *Proc. Natl. Acad. Sci. USA* **2012**, *109*, 10012.
[79] T. Minas, A. H. Gomoll, R. Rosenberger, R. O. Royce, T. Bryant, *Am. J. Sports Med.* **2009**, *37*, 902.
[80] Y. Zhang, L. Ye, J. Cui, B. Yang, H. Sun, J. Li, F. Yao, *ACS Biomater. Sci. Eng.* **2016**, *2*, 544.
[81] A. F. Girão, Â. Semitela, A. L. Pereira, A. Completo, P. A. A. P. Marques, *J. Mater. Sci. Mater. Med.* **2020**, *31*, 69.
[82] T. Guo, J. Lembong, L. G. Zhang, J. P. Fisher, *Tissue Eng. Part B Rev.* **2017**, *23*, 225.
[83] M. Castilho, V. Mouser, M. Chen, J. Malda, K. Ito, *Acta Biomater.* **2019**, *95*, 297.
[84] N. Munir, A. McDonald, A. Callanan, *Bioprinting* **2019**, *16*, e00056.
[85] Â. Semitela, A. F. Girão, C. Fernandes, G. Ramalho, S. C. Pinto, A. Completo, P. A. A. P. Marques, *J. Mech. Behav. Biomed. Mater.* **2021**, *117*, 104373.
[86] Â. Semitela, A. F. Girão, C. Fernandes, G. Ramalho, I. Bdikin, A. Completo, P. A. A. P. Marques, *J. Biomater. Appl.* **2020**, *35*, 471.
[87] Y. Cao, P. Cheng, S. Sang, C. Xiang, Y. An, X. Wei, Z. Shen, Y. Zhang, P. Li, *Regen. Biomater.* **2021**, *8*, rbab019.
[88] A. F. Girão, Â. Semitela, G. Ramalho, A. Completo, P. A. A. P. Marques, *Compos. B: Eng.* **2018**, *154*, 99.
[89] A. Tampieri, M. Sandri, E. Landi, D. Pressato, S. Francioli, R. Quarto, I. Martin, *Biomaterials* **2008**, *29*, 3539.
[90] C. Gegg, F. Yang, *Acta Biomater.* **2020**, *101*, 196.
[91] S. J. Wang, Z. Z. Zhang, D. Jiang, Y. S. Qi, H. J. Wang, J. Y. Zhang, J. X. Ding, J. K. Yu, *Polymers* **2016**, *8*, 200.
[92] H. Liu, Y. Cheng, J. Chen, F. Chang, J. Wang, J. Ding, X. Chen, *Acta Biomater.* **2018**, *73*, 103.
[93] Y. Zhang, J. Zhang, F. Chang, W. Xu, J. Ding, *Mater. Sci. Eng. C* **2018**, *88*, 79.
[94] Y. Zhang, J. Yu, K. Ren, J. Zuo, J. Ding, X. Chen, *Biomacromolecules* **2019**, *20*, 1478.
[95] J. Yang, Y. Li, Y. Liu, D. Li, L. Zhang, Q. Wang, Y. Xiao, X. Zhang, *Acta Biomater.* **2019**, *91*, 159.
[96] J. K. Wise, A. L. Yarin, C. M. Megaridis, M. Cho, *Tissue Eng Part A* **2009**, *15*, 913.
[97] S. Jahn, J. Klein, *Phys. Today* **2018**, *71*, 48.
[98] S. Camarero-Espinosa, B. Rothen-Rutishauser, C. Weder, E. J. Foster, *Biomaterials* **2016**, *74*, 42.
[99] Y. Wu, Z. Yang, J. B. K. Law, A. Y. He, A. A. Abbas, V. Denslin, T. Kamarul, J. H. P. Hui, E. H. Lee, *Tissue Eng. Part A* **2017**, *23*, 43.
[100] Y. N. Wu, J. B. K. Law, A. Y. He, H. Y. Low, J. H. P. Hui, C. T. Lim, Z. Yang, E. H. Lee, *Nanomedicine* **2014**, *10*, 1507.
[101] J. C. Mansfield, J. S. Bell, C. P. Winlove, *Osteoarthritis Cartilage* **2015**, *23*, 1806.
[102] F. H. Silver, G. Bradica, A. Tria, *Matrix Biol.* **2002**, *21*, 129.
[103] S. Ghassemi, G. Meacci, S. Liu, A. A. Gondarenko, A. Mathur, P. Roca-Cusachs, M. P. Sheetz, J. Hone, *Proc. Natl. Acad. Sci. USA* **2012**, *109*, 5328.
[104] J. Fu, Y. K. Wang, M. T. Yang, R. A. Desai, X. Yu, Z. Liu, C. S. Chen, *Nat. Methods* **2010**, *7*, 733.
[105] J. A. M. Steele, S. D. McCullen, A. Callanan, H. Autefage, M. A. Accardi, D. Dini, M. M. Stevens, *Acta Biomater.* **2014**, *10*, 2065.
[106] F. Bothe, A. K. Deubel, E. Hesse, B. Lotz, J. Groll, C. Werner, W. Richter, S. Hagmann, *Int. J. Mol. Sci.* **2019**, *20*, 653.
[107] T. M. McCarrel, S. L. Pownder, S. Gilbert, M. F. Koff, E. Castiglione, R. A. Saska, G. Bradica, L. A. Fortier, *Cartilage* **2017**, *8*, 406.
[108] J. P. K. Armstrong, E. Pchelintseva, S. Treumuth, C. Campanella, C. Meinert, T. J. Klein, D. W. Hutmacher, B. W. Drinkwater, M. M. Stevens, *Adv. Healthcare Mater.* **2022**, *11*, 2200481.
[109] A. S. A. Eskelinen, P. Tanska, C. Florea, G. A. Orozco, P. Julkunen, A. J. Grodzinsky, R. K. Korhonen, *PLoS Comput. Biol.* **2020**, *16*, e1007998.
[110] L. Fu, P. Li, H. Li, C. Gao, Z. Yang, T. Zhao, W. Chen, Z. Liao, Y. Peng, F. Cao, X. Sui, S. Liu, Q. Guo, *Stem Cells Int.* **2021**, *2021*, 6621806.
[111] G. A. Ateshian, *J. Biomech.* **2009**, *42*, 1163.
[112] G. Friedl, H. Schmidt, I. Rehak, G. Kostner, K. Schauenstein, R. Windhager, *Osteoarthritis Cartilage* **2007**, *15*, 1293.
[113] X. Huang, R. Das, A. Patel, T. D. Nguyen, *Regen. Eng. Transl. Med.* **2018**, *4*, 216.
[114] Z. Yang, Y. Wu, L. Yin, H. L. Eng, in *Advances in Biomechanics and Tissue Regeneration* (Ed: M. H. Doweidar), Elsevier, New York **2019**, pp. 379–392.
[115] S. Balko, J. F. Weber, S. D. Waldman, in *Orthopedic Biomaterials: Progress in Biology, Manufacturing, and Industry Perspectives*, (Eds: B. Li, T. Webster), Springer International Publishing, Cham **2018**, p. 123.
[116] A. Savadipour, R. J. Nims, D. B. Katz, F. Guilak, *Connect. Tissue Res.* **2022**, *63*, 69.
[117] K. Gavenis, C. Schumacher, U. Schneider, J. Eisfeld, J. Mollenhauer, B. Schmidt-Rohlfing, *Mol. Cell. Biochem.* **2009**, *321*, 135.
[118] G. Du, L. Li, X. Zhang, J. Liu, J. Hao, J. Zhu, H. Wu, W. Chen, Q. Zhang, *Exp. Biol. Med.* **2020**, *245*, 180.
[119] M. A. Soltz, G. A. Ateshian, *J. Biomech.* **1998**, *31*, 927.
[120] B. D. Elder, K. A. Athanasiou, *Tissue Eng. Part B Rev.* **2009**, *15*, 43.
[121] Y. Li, J. Zhou, X. Yang, Y. Jiang, J. Gui, *Dev. Growth Differ.* **2016**, *58*, 180.
[122] C. Schröder, A. Hölzer, G. Zhu, M. Woiczinski, O. B. Betz, H. Graf, S. Mayer-Wagner, P. E. Müller, *J. Mech. Med. Biol.* **2016**, *16*, 1650025.
[123] A. Nazempour, C. R. Quisenberry, N. I. Abu-Lail, B. J. van Wie, *Cell Tissue Res.* **2017**, *370*, 179.
[124] A. Nazempour, C. R. Quisenberry, B. J. van Wie, N. I. Abu-Lail, *J. Nanosci. Nanotechnol.* **2016**, *16*, 3136.
[125] T. I. Morales, A. B. Roberts, *J. Biol. Chem.* **1988**, *263*, 12828.
[126] N. Shintani, E. B. Hunziker, *Eur. Cell Mater.* **2011**, *22*, 302.
[127] L. F. Mellor, A. J. Steward, R. C. Nordberg, M. A. Taylor, E. G. Loboa, *Aerosp. Med. Hum. Perform.* **2017**, *88*, 377.
[128] J. Meng, X. Ma, D. Ma, C. Xu, *Osteoarthritis Cartilage* **2005**, *13*, 1115.
[129] J. de Boer, R. Siddappa, C. Gaspar, A. van Apeldoorn, R. Fodde, C. van Blitterswijk, *Bone* **2004**, *34*, 818.
[130] Y. Usami, A. T. Gunawardena, M. Iwamoto, M. Enomoto-Iwamoto, *Lab. Invest.* **2016**, *96*, 186.
[131] J. Chen, Z. Yuan, Y. Liu, R. Zheng, Y. Dai, R. Tao, H. Xia, H. Liu, Z. Zhang, W. Zhang, W. Liu, Y. Cao, G. Zhou, *Stem Cells Transl. Med.* **2017**, *6*, 982.
[132] Y. Wu, L. Zhu, H. Jiang, W. Liu, Y. Liu, Y. Cao, G. Zhou, *JPRAS Open* **2010**, *63*, e370.
[133] S. Ansari, A. Karkhaneh, S. Bonakdar, N. Haghighipour, *Eur. Polym. J.* **2019**, *118*, 244.
[134] P. Aprile, D. J. Kelly, *Front. Bioeng. Biotechnol.* **2021**, *8*, 619914.
[135] N. Sawatjui, T. Limpaiboon, K. Schrobback, T. Klein, *J. Tissue Eng. Regen. Med.* **2018**, *12*, 1220.
[136] W. Wang, Y. Wan, T. Fu, T. Zhou, X. Tang, H. Wu, C. Liu, M. Jagodzinski, *J. Biomed. Mater. Res., Part A* **2019**, *107*, 1294.
[137] A. C. Daly, D. J. Kelly, *Biomaterials* **2019**, *197*, 194.
[138] T. Mesallati, E. J. Sheehy, T. Vinardell, C. T. Buckley, D. J. Kelly, *Eur. Cell Mater.* **2015**, *30*, 163.
[139] S. D. Thorpe, T. Nagel, S. F. Carroll, D. J. Kelly, *PLoS One* **2013**, *8*, e60764.
[140] L. Luo, A. R. O'Reilly, S. D. Thorpe, C. T. Buckley, D. J. Kelly, *J. Tissue Eng. Regen. Med.* **2017**, *11*, 2613.
[141] D. P. Burke, H. Khayyeri, D. J. Kelly, *Biomech. Model. Mechanobiol.* **2015**, *14*, 93.
[142] P. Malaviya, R. M. Nerem, *Tissue Eng.* **2002**, *8*, 581.
[143] T. W. G. M. Spitters, J. C. H. Leijten, F. D. Deus, I. B. F. Costa, A. A. van Apeldoorn, C. A. van Blitterswijk, M. Karperien, *Tissue Eng. Part C: Methods* **2013**, *19*, 774.

[144] K. S. Furukawa, K. Imura, T. Tateishi, T. Ushida, *J. Biotechnol.* **2008**, *133*, 134.
[145] C. V. Gemmiti, R. E. Guldberg, *Biotechnol. Bioeng.* **2009**, *104*, 809.
[146] S. D. Waldman, C. G. Spiteri, M. D. Grynpas, R. M. Pilliar, R. A. Kandel, *J. Orthop. Res.* **2003**, *21*, 590.
[147] C. Lee, S. Grad, M. Wimmer, M. Alini, in *Topics in Tissue Engineering*, (Eds: N. Ashammakhi, R. L. Reis), Oulu University, Finland **2006**, pp. 1–32.
[148] K. Lagana, M. Moretti, G. Dubini, M. T. Raimondi, *Proc. Inst. Mech. Eng., Part H* **2008**, *222*, 705.
[149] M. M. Nava, M. T. Raimondi, R. Pietrabissa, *Biomech. Model. Mechanobiol.* **2013**, *12*, 1169.
[150] E. DiFederico, J. C. Shelton, D. L. Bader, *Biotechnol. Bioeng.* **2017**, *114*, 1614.
[151] I. S. Park, W. H. Choi, D. Y. Park, S. R. Park, S. H. Park, B. H. Min, *PLoS One* **2018**, *13*, e0202834.
[152] M. L. Vainieri, D. Wahl, M. Alini, G. J. V. M. van Osch, S. Grad, *Acta Biomater.* **2018**, *81*, 256.
[153] C. Meinert, K. Schrobback, D. W. Hutmacher, T. J. Klein, *Sci. Rep.* **2017**, *7*, 16997.
[154] T. Ogura, T. Minas, A. Tsuchiya, S. Mizuno, *J. Tissue Eng. Regen. Med.* **2019**, *13*, 1143.
[155] C. A. Tee, Z. Yang, L. Yin, Y. Wu, J. Han, E. H. Lee, *Biomaterials* **2019**, *220*, 119409.
[156] C. A. Tee, Z. Yang, Y. Wu, X. Ren, M. Baranski, D. J. Lin, A. Hassan, J. Han, E. H. Lee, *Cartilage* **2022**, *13*, 194760352210930.
[157] T. Chen, M. J. Hilton, E. B. Brown, M. J. Zuscik, H. A. Awad, *Biotechnol. Bioeng.* **2012**, *110*, 1476.
[158] R. L. Smith, M. C. D. Trindade, T. Ikenoue, M. Mohtai, P. Das, D. R. Carter, S. B. Goodman, D. J. Schurman, *Biorheology* **2000**, *37*, 95.
[159] Z. R. Healy, F. Zhu, J. D. Stull, K. Konstantopoulos, *Am. J. Physiol. Cell Physiol.* **2008**, *294*, C1146.
[160] C. M. Begley, S. J. Kleis, *Biotechnol. Bioeng.* **2000**, *70*, 32.
[161] E. Y. Salinas, A. Aryaei, N. Paschos, E. Berson, H. Kwon, J. C. Hu, K. A. Athanasiou, *Biofabrication* **2020**, *12*, 045010.
[162] X. Ren, F. Wang, C. Chen, X. Gong, L. Yin, L. Yang, *BMC Musculoskelet. Disord.* **2016**, *17*, 301.
[163] K. Schrobback, J. Malda, R. W. Crawford, Z. Upton, D. I. Leavesley, T. J. Klein, *Tissue Eng. Part A* **2012**, *18*, 920.
[164] T. W. G. M. Spitters, C. M. D. Mota, S. C. Uzoechi, B. Slowinska, D. E. Martens, L. Moroni, M. Karperien, *Tissue Eng. Part A* **2014**, *20*, 3270.
[165] K. L. Collins, E. M. Gates, C. L. Gilchrist, B. D. Hoffman, in *Bio-Instructive Scaffolds for Musculoskeletal Tissue Engineering and Regenerative Medicine*, (Eds: J. L. Brown, B. L. Banik, S. G. Kumbar), Elsevier, New York **2017**, pp. 3–35.
[166] K. E. Wescoe, R. C. Schugar, C. R. Chu, B. M. Deasy, *Cell Biochem. Biophys.* **2008**, *52*, 85.
[167] X. Wang, E. Wenk, X. Zhang, L. Meinel, G. Vunjak-Novakovic, D. L. Kaplan, *J. Controlled Release* **2009**, *134*, 81.
[168] S. Moeinzadeh, M. Monavarian, S. Kader, E. Jabbari, *Tissue Eng. Part A* **2019**, *25*, 234.
[169] V. J. Bianchi, A. Lee, J. Anderson, J. Parreno, J. Theodoropoulos, D. Backstein, R. Kandel, *Am. J. Sports Med.* **2019**, *47*, 2348.
[170] T. Zhu, M. Jiang, M. Zhang, L. Cui, X. Yang, X. Wang, G. Liu, J. Ding, X. Chen, *Bioact. Mater.* **2022**, *9*, 446.
[171] T. Zhu, M. Jiang, M. Zhang, L. Cui, X. Yang, X. Wang, G. Liu, J. Ding, X. Chen, *MethodsX* **2022**, *9*, 101713.
[172] S. Diederichs, Y. Renz, S. Hagmann, B. Lotz, E. Seebach, W. Richter, *J. Biomed. Mater. Res. B Appl. Biomater.* **2018**, *106*, 2214.
[173] M. Demoor, D. Ollitrault, T. Gomez-Leduc, M. Bouyoucef, M. Hervieu, H. Fabre, J. Lafont, J. M. Denoix, F. Audigié, F. Mallein-Gerin, F. Legendre, P. Galera, *Biochim. Biophys. Acta Gen. Subj.* **2014**, *1840*, 2414.
[174] W. D. Lee, M. B. Hurtig, R. M. Pilliar, W. L. Stanford, R. A. Kandel, *Osteoarthritis Cartilage* **2015**, *23*, 1307.
[175] N. T. Khanarian, N. M. Haney, R. A. Burga, H. H. Lu, *Biomaterials* **2012**, *33*, 5247.
[176] N. Fahy, O. F. W. Gardner, M. Alini, M. J. Stoddart, *Tissue Eng. Part A* **2018**, *24*, 849.
[177] J. C. Silva, R. N. Udangawa, J. Chen, C. D. Mancinelli, F. F. F. Garrudo, P. E. Mikael, J. M. S. Cabral, F. C. Ferreira, R. J. Linhardt, *Mater. Sci. Eng. C* **2020**, *107*, 110291.
[178] J. Wang, Y. Wang, X. Sun, D. Liu, C. Huang, J. Wu, C. Yang, Q. Zhang, *Artif. Cells Nanomed. Biotechnol.* **2019**, *47*, 1710.
[179] X. Li, J. Ding, Z. Zhang, M. Yang, J. Yu, J. Wang, F. Chang, X. Chen, *ACS Appl. Mater. Interfaces* **2016**, *8*, 5148.
[180] D. Dehghan-Baniani, B. Mehrjou, D. Wang, R. Bagheri, A. Solouk, P. K. Chu, H. Wu, *Int. J. Biol. Macromol.* **2022**, *205*, 638.
[181] Y. Shi, X. Hu, J. Cheng, X. Zhang, F. Zhao, W. Shi, B. Ren, H. Yu, P. Yang, Z. Li, Q. Liu, Z. Liu, X. Duan, X. Fu, J. Zhang, J. Wang, Y. Ao, *Nat. Commun.* **2019**, *10*, 1914.
[182] E. Choi, J. Lee, S. Lee, B.-W. Song, H.-H. Seo, M.-J. Cha, S. Lim, C. Lee, S.-W. Song, G. Han, K.-C. Hwang, *Bioorg. Med. Chem. Lett.* **2016**, *26*, 5098.
[183] R. Shkhyan, B. Van Handel, J. Bogdanov, S. Lee, Y. Yu, M. Scheinberg, N. W. Banks, S. Limfat, A. Chernostrik, C. E. Franciozi, M. P. Alam, V. John, L. Wu, G. B. Ferguson, A. Nsair, F. A. Petrigliano, C. T. Vangsness, K. Vadivel, P. Bajaj, L. Wang, N. Q. Liu, D. Evseenko, *Ann. Rheum. Dis.* **2018**, *77*, 760.
[184] T. Li, B. Liu, K. Chen, Y. Lou, Y. Jiang, D. Zhang, *Biomed. Pharmacother.* **2020**, *131*, 110652.
[185] J. E. Barthold, K. P. McCreery, J. Martinez, C. Bellerjeau, Y. Ding, S. J. Bryant, G. L. Whiting, C. P. Neu, *Biofabrication* **2022**, *14*, 025021.
[186] X. Nie, Y. J. Chuah, W. Zhu, P. He, Y. Peck, D. A. Wang, *Biomaterials* **2020**, *235*, 119821.
[187] L. Luo, J. Y. J. Chu, R. Eswaramoorthy, K. J. Mulhall, D. J. Kelly, *ACS Biomater. Sci. Eng.* **2017**, *3*, 1933.
[188] L. H. Nguyen, A. K. Kudva, N. L. Guckert, K. D. Linse, K. Roy, *Biomaterials* **2011**, *32*, 1327.
[189] L. H. Nguyen, A. K. Kudva, N. S. Saxena, K. Roy, *Biomaterials* **2011**, *32*, 6946.
[190] T. Lam, T. Dehne, J. P. Krüger, S. Hondke, M. Endres, A. Thomas, R. Lauster, M. Sittinger, L. Kloke, *J. Biomed. Mater. Res. B: Appl. Biomater.* **2019**, *107*, 2649.
[191] K. Parratt, M. Smerchansky, Q. Stiggers, K. Roy, *J. Mater. Chem. B* **2017**, *5*, 6237.
[192] H. A. Owida, R. Yang, L. Cen, N. J. Kuiper, Y. Yang, *J. R. Soc. Interface* **2018**, *15*, 20180310.
[193] D. Clearfield, A. Nguyen, M. Wei, *J. Biomed. Mater. Res., Part A* **2018**, *106*, 948.
[194] X. F. Zheng, S. B. Lu, W. G. Zhang, S. Y. Liu, J. X. Huang, Q. Y. Guo, *Biotechnol. Bioprocess Eng.* **2011**, *16*, 593.
[195] S. P. Grogan, X. Chen, S. Sovani, N. Taniguchi, C. W. Colwell, M. K. Lotz, D. D. D'Lima, *Tissue Eng. Part A* **2014**, *20*, 264.
[196] V. H. M. Mouser, R. Levato, A. Mensinga, W. J. A. Dhert, D. Gawlitta, J. Malda, *Connect. Tissue Res.* **2020**, *61*, 137.
[197] J. Idaszek, M. Costantini, T. A. Karlsen, J. Jaroszewicz, C. Colosi, S. Testa, E. Fornetti, S. Bernardini, M. Seta, K. Kasarełło, R. Wrzesień, S. Cannata, A. Barbetta, C. Gargioli, J. E. Brinchman, W. Święszkowski, *Biofabrication* **2019**, *11*, 044101.
[198] A. Dimaraki, P. J. DÃ-Az-Payno, M. Minneboo, M. Nouri-Goushki, M. Hosseini, N. Kops, R. Narcisi, M. J. Mirzaali, G. J. V. M. Van Osch, L. E. Fratila-Apachitei, A. A. Zadpoor, *Appl. Sci.* **2021**, *11*, 7821.
[199] A. Kosik-Kozioł, M. Costantini, A. Mróz, J. Idaszek, M. Heljak, J. Jaroszewicz, E. Kijeńska, K. Szöke, N. Frerker, A. Barbetta, J. E. Brinchman, W. Święszkowski, *Biofabrication* **2019**, *11*, 035016.

[200] G. M. Cunniffe, P. J. Díaz-Payno, E. J. Sheehy, S. E. Critchley, H. V. Almeida, P. Pitacco, S. F. Carroll, O. R. Mahon, A. Dunne, T. J. Levingstone, C. J. Moran, R. T. Brady, F. J. O'brien, P. A. J. Brama, D. J. Kelly, *Biomaterials* **2019**, *188*, 63.
[201] E. Kunisch, A. K. Knauf, E. Hesse, U. Freudenberg, C. Werner, F. Bothe, S. Diederichs, W. Richter, *Biofabrication* **2019**, *11*, 015001.
[202] U. Schneider, L. Rackwitz, S. Andereya, S. Siebenlist, F. Fensky, J. Reichert, I. Löer, T. Barthel, M. Rudert, U. Nöth, *Am. J. Sports Med.* **2011**, *39*, 2558.
[203] S. Trattnig, K. Pinker, C. Krestan, C. Plank, S. Millington, S. Marlovits, *Eur. J. Radiol.* **2006**, *57*, 9.
[204] P. C. Kreuz, S. Müller, U. Freymann, C. Erggelet, P. Niemeyer, C. Kaps, A. Hirschmüller, *Am. J. Sports Med.* **2011**, *39*, 1697.
[205] P. Hindle, J. L. Hendry, J. F. Keating, L. C. Biant, *Knee Surg. Sports Traumatol. Arthrosc.* **2014**, *22*, 1235.
[206] H. Binder, L. Hoffman, L. Zak, T. Tiefenboeck, S. Aldrian, C. Albrecht, C. Albrecht, *Bone Jt. Res.* **2021**, *10*, 370.
[207] K. B. McGowan, G. Stiegman, *Cartilage* **2013**, *4*, 4.
[208] V. Horbert, L. Xin, P. Foehr, O. Brinkmann, M. Bungartz, R. H. Burgkart, T. Graeve, R. W. Kinne, *Cartilage* **2019**, *10*, 346.
[209] T. Nagel, D. J. Kelly, *Tissue Eng. Part A* **2013**, *19*, 824.
[210] J. Iwasa, L. Engebretsen, Y. Shima, M. Ochi, *Knee Surg. Sports Traumatol. Arthrosc.* **2009**, *17*, 561.
[211] B. Sridharan, B. Sharma, M. S. Detamore, *Tissue Eng. Part B Rev.* **2016**, *22*, 15.
[212] R. Stoop, *Injury* **2008**, *39*, 77.
[213] N. Eslahi, M. Abdorahim, A. Simchi, *Biomacromolecules* **2016**, *17*, 3441.
[214] I. F. Cengiz, H. Pereira, L. de Girolamo, M. Cucchiarini, J. Espregueira-Mendes, R. L. Reis, J. M. Oliveira, *J. Exp. Orthop.* **2018**, *5*, 14.

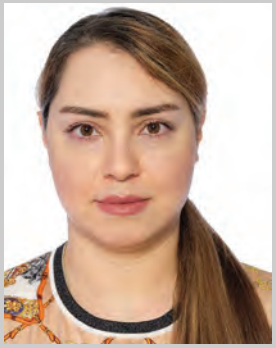

Dorsa Dehghan-Baniani received her Ph.D. in both materials science and engineering and biomedical engineering at 2019 from Sharif University of Technology and The Hong Kong University of Science and Technology on polymeric biomaterials for cartilage tissue engineering. She is now a postdoctoral fellow in the Department of Orthopaedics and Traumatology of The Chinese University of Hong Kong and her research interests include developing polymeric biomaterials and implants based on tissue derived extracellular matrix, silk, chitosan, etc., for applications such as wound, bone, and cartilage tissue engineering with advanced methods like droplet microfluidics, 3D printing, etc.

Babak Mehrjou received his Ph.D. in materials science and engineering in 2020 from City University of Hong Kong on biomimicked silk-based antibacterial surface and its application on corrosion improvement of magnesium alloy. He is now a postdoctoral fellow in the Department of Physics of City University of Hong Kong and his research interests include design of antibacterial surfaces, biopolymers, plasma surface treatment of biomaterials, metal organic frameworks, corrosion improvement of bio-metallics, and cartilage tissue engineering.

Paul K. Chu received his B.S. in mathematics from The Ohio State University and M.S./Ph.D. in chemistry from Cornell University. He is Chair Professor of Materials Engineering in City University of Hong Kong. His research activities are quite diverse spanning plasma and materials science and engineering. He is a highly cited researcher and has received more than 20 scientific/technical awards. He is a fellow of the APS, AVS, IEEE, MRS, and HKIE. He is also a fellow and council member of the Hong Kong Academy of Engineering Sciences (HKAES).

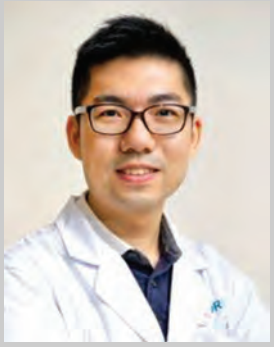

Wayne Yuk Wai Lee obtained his Ph.D. in pharmacology from The Chinese University of Hong Kong (CUHK) in 2009. Currently, he is an assistant professor in the Department of Orthopaedics and Traumatology, CUHK. He has published over 100 publications in peer-reviewed international journals (Scopus H-index 31). One of his research interests focuses on the development of GMP-grade advanced therapy products to treat osteoarthritis and other musculoskeletal problems. He is also a registered authorized person for advanced therapy products in Hong Kong. His team also explore novel treatment strategies such as MSC secretome, miRNA, and biomaterials with MSC tracking and controlled release properties.

Hongkai Wu received his B.Sc. and M.Sc. in chemistry at University of Science and Technol of China in 1995 and 1997, respectively, and Ph.D. degree in chemistry from Harvard University in 2002. After his postdoctoral training at Stanford University, he joined Tsinghua University in 2005 and moved to the Hong Kong University of Science and Technology in 2007. He is currently a professor in the Department of Chemistry (affiliated with the Department of Chemical and Biological Engineering) at the Hong Kong University of Science and Technology. His research interests are focused on the interdisciplinary frontiers of microfluidics, bioanalytical science, and biomaterials.